Atmospheric Research 222 (2019) 134–153

Contents lists available at ScienceDirect

Atmospheric Research

journal homepage: www.elsevier.com/locate/atmosres

Changes in precipitation extremes in the Beijing metropolitan area during 1960–2012

Xiaomeng Song[a,b,c,*], Jianyun Zhang[b], Xianju Zou[a], Chunhua Zhang[a], Amir AghaKouchak[d], Fanzhe Kong[a]

[a] School of Resources and Geosciences, China University of Mining & Technology, Xuzhou 221116, China
[b] State Key Laboratory of Hydrology-Water Resources and Hydraulic Engineering, Nanjing Hydraulic Research Institute, Nanjing 210029, China
[c] State Key Laboratory of Water Resources and Hydropower Engineering Science, Wuhan University, Wuhan 430072, China
[d] Center for Hydrometeorology and Remote Sensing, University of California, Irvine, CA 92697, USA

ARTICLE INFO

Keywords:
Extreme precipitation
Entropy-based method
Climate change
Urban effect
Wavelet transform coherence method
Beijing area

ABSTRACT

In this study, we use several methods including the minimum cross entropy, wavelet transform coherence method, and the Mann-Kendall test to study the changes in the frequency of precipitation extremes and their contributions to total precipitation at different extreme percentile thresholds (90th percentile, 95th percentile, and 99th percentile) in the Beijing metropolitan area. Overall, the spatial distribution of the extreme precipitation thresholds is consistent with that of total precipitation, with the highest distribution appearing in the northeast part of the study area and the lowest distribution appearing in the west. The extreme precipitation events with high-percentile thresholds have more spatial and temporal variability than those at the low-percentile thresholds. We consider two types of indices representing frequency of extremes and their contributions to total precipitation. The frequency indices show similar spatial and temporal trends relative to the total precipitation than the contribution ratio indices. Additionally, the possible impacts of global climate indices, urban expansion and topography on the change in precipitation extremes are also considered. The weakening Eastern Asian monsoon (EAM) since 1970s has significantly influenced the change in contribution from indices of extreme precipitation over Beijing. The changes in precipitation extremes are also influenced by rapid urban expansion and topography, especially in spatial changes, with the higher values appearing in the urban and plain areas. In the context of global climate change and rapid urbanization, greater challenges in urban flooding and safety are caused by the changes in precipitation extremes.

1. Introduction

There is a broad recognition that global climate is changing over history, not only generally referring to global warming, but also extreme events, which are projected to increase in intensity and magnitude (Janssen et al., 2016; Kunkel et al., 2012; Pakalidou and Karacosta, 2018). Generally, extreme events have a large potential to cause significant damage to agriculture, ecology, and infrastructure, as well as disrupt economic activities and lead to the loss of human life. As a result, their characteristics and any change or trend thereof have attracted a great deal of attention (Allan and Soden, 2008; Cheng et al., 2014; Easterling et al., 2000; Hao et al., 2013; Lenderink and Van Meijgaard, 2008; Liang and Ding, 2017; Min et al., 2011; Yang and Smith, 2018; Zhai et al., 2005). In recently years, many extreme precipitation events have taken place around the world, and they have caused serious impacts on the human society and ecological environment (Wu and Lau, 2016). For example, in 2017 alone, the United States experienced four major flooding events from extreme precipitation, resulting in 211 deaths and over 180 billion dollars in damages (Touma et al., 2018). Understanding the spatial characteristics of these extreme precipitation events is important not only because of their considerable social impacts, but also because these characteristics have been changing in recent decades as atmospheric temperatures increase (Touma et al., 2018). Therefore, numerous studies have investigated the trends and variability of precipitation extremes around the world or in the special regions (Cavalcanti, 2012; Goswami et al., 2018; Sun et al., 2016; Tabari and Willems, 2018; Thapa et al., 2018; Tong et al., 2019; Wibig and Piotrowski, 2018; Xie et al., 2018; Zarekarizi et al.,

* Corresponding author at: Institute of Hydrology and Water Resources, School of Resources and Geosciences, China University of Mining & Technology, Daxue Road No.1, Xuzhou 221116, China.
E-mail address: xmsong@cumt.edu.cn (X. Song).

https://doi.org/10.1016/j.atmosres.2019.02.006
Received 17 October 2018; Received in revised form 14 February 2019; Accepted 14 February 2019
Available online 26 February 2019
0169-8095/

2018).

Extreme precipitation events often pose more complex short-term challenges than analyzing annual or seasonal precipitation amount and variability (AghaKouchak, 2014; Gao et al., 2016). For instance, non-stationary patterns have been observed in many climate records, especially in the second half of the 20th century (AghaKouchak et al., 2011; Cheng and AghaKouchak, 2014). Yet the trend of those extreme events is too complex to offer a clear picture (Alexander et al., 2006; Donat et al., 2016; Frich et al., 2002). For example, since approximately the 1950s, while more in-land areas in the world (e.g., North and Central America, southern Europe, East Asia, and Mediterranean region) have witnessed an increasing number of heavy or extreme precipitation events(Zolina et al., 2014), other areas (e.g., North China, Australia, eastern Germany) have seen the opposite (Han et al., 2015; Zhai et al., 2005). Even at smaller spatial scales, substantial heterogeneity in extreme precipitation distribution and their trend is evident; largely due to complex climate dynamics and their interaction with many other factors, including human activities, land-use change, and urbanization, as observed by Feng et al. (2014) in the case of China. A series of related studies also revealed the dramatic contrasts in extreme precipitation trends in different parts of the country: While an increasing trend has been found in the Yangtze River basin, southeastern and northwestern China as well as the southern and northern Tibetan Plateau; the Yellow River basin, northern China, and the central Tibetan Plateau observe reducing occurrences (Chen and Zhai, 2013; Damberg and AghaKouchak, 2014; Dong et al., 2011; Gao et al., 2018; Gao et al., 2017; Wang et al., 2008b; Wang and Zhou, 2005; Yao et al., 2010; Zheng et al., 2006; Zhou and Lei, 2018).

Climate change can exert profound stresses on urban environments, which are sensitive to extreme meteorological events (Ali and Mishra, 2018; Georgescu et al., 2014) because urban areas are centers of wealth, human population and built infrastructure (Willems, 2013). Generally, urban areas are considered by some to be “first responders” to climate change (Rosenzweig et al., 2010), and are the fundamental units for climate change mitigation and adaptation (Georgescu et al., 2014), with increasing flooding risk (Hallegatte et al., 2013). It is of great value and necessity to investigate the changes of precipitation extremes (e.g., intensity, frequency) and their possible variations associated with climate change's impacts, particularly in metropolitan areas. Additionally, through this investigation, one gains an enhanced understanding of extreme precipitation processes and possible anthropogenic or natural causes of change. In the recent past, extreme precipitation events, which cause disproportionate damage to urban transportation system and pose challenges to urban stormwater drainage systems (Mishra et al., 2012), have affected many large urban areas including Beijing (2012), Bangkok (2011), Brisbane (2011), Guangzhou (2007), Mumbai (2005) and Washington DC (2005). For example, the Beijing metropolitan area is socio-economically vulnerable to extreme precipitation events and associated flooding due to global climate change and intense human activity, as observed during the event of July 21, 2012 (Zhao et al., 2014a; Zhao et al., 2013). Therefore, the changes in extreme events in urban areas have become a hotspot issue for hydrologists and meteorologists. For example, Kishtawal et al. (2010) found that increase in trend of extreme precipitation was significantly higher in urban than in rural areas by analyzing in situ and satellite-based precipitation and population datasets. Ali et al. (2014) examined changes in extreme precipitation over 57 major urban areas in India under the observed (1901–2010) and projected future climate (2010–2060). Pingale et al. (2014) analyzed the trends in extreme annual daily precipitation for 1971–2005 in 33 urban areas in Rajasthan arid and semi-arid regions of India and found negative trends in annual rainfall and extreme annual daily precipitation in most of the cities. Mishra et al. (2015) discussed the climate extremes including temperature and precipitation extremes, using observed station data for 217 urban areas across the globe during the period of 1973–2012. They found that significant increases in the frequency of daily precipitation extreme and in annual maximum precipitation only occurred at smaller fractions (17% and 10% respectively) of the total urban areas. Li et al. (2015) discussed the changes of precipitation and extremes based on daily precipitation at 15 stations in Beijing with the homogenization method. Zhang et al. (2015) addressed the precipitation frequency under nonstationary conditions based on the 12 stations in Beijing-Tianjin-Hebei region of China. Siswanto et al. (2016) emphasized that the extreme precipitation in Jakarta exhibited a positive trend over the 1866–2010 period with an even stronger trend over the period of 1961–2010 based on long-term observed records. Zhou et al. (2017) noted that the extreme precipitation for all the cities in Jing-Jin-Ji (Beijing-Tianjin-Hebei) City Cluster had a decreasing trend while an increasing trend in the Yangtze City Cluster by analyzing the trends in extreme precipitation in 146 cities in China during 1960–2014. Liang and Ding (2017) found that extreme hourly precipitation events had a significantly increasing trend during the period of 1916–2014, and the urbanization in Shanghai contributed greatly to the increase in both frequency and intensity of extreme precipitation. Thus, especially in urban areas, it is very important to understand how and why precipitation extremes have changed in the past as well as how they will change in the future. Another problem is how changes in precipitation extremes can affect urban flooding and urban water security management.

To extend the many existing studies in this field, this work focuses on examining spatial and temporal changes in precipitation extremes in Beijing and attempts to provide a more comprehensive picture of extreme precipitation events in the region. Toward this end, we use high-quality daily data from a relatively dense rain-gauge network in Beijing during 1960–2012. Additionally, this study aims to analyze the frequency and magnitude of extreme precipitation events, both temporally and spatially, and attempts to discuss the possible causes and implications for urban flooding. The paper is organized as follows: We describe the data and methods in section 2, including detailed descriptions of the sources of daily data, definitions of the indices and analysis methods. Results are presented in section 3. We also offer some discussion of the results in section 3 followed by conclusions in section 4.

2. Data and methods

2.1. Study area and data set

2.1.1. Brief description of the study area

Beijing, located in the North China Plain, is one of the most populous cities in the world (Fig. 1). The main city lies on flat land surrounded by mountains from the southwest to the northeast. Beijing has a monsoon-driven humid continental climate, characterized by hot humid summers and cold dry winters (Song et al., 2014). Generally, Beijing belongs to a sub-humid and sub-arid region, with a mean annual precipitation around 600 mm. However, since 2000, the annual precipitation has significantly decreased to < 500 mm (Song et al., 2014), while extreme precipitation events have been widely reported with abominable effects on human activities and the economy of the region. As a result, we selected the Beijing metropolitan area as the study area.

2.1.2. Precipitation data

The main dataset for this study is daily precipitation records collected from 60 rain-gauge stations located in the study area (Fig. 1) and covering 1960–2012. These records are mainly supplied by the Beijing Hydrological Center (BHC) of the Beijing Water Authority with some exceptions extracted from the *Annual Hydrological Report: Hydrological Data of Haihe River Basin*. All data has been subjected to vigorous quality-control procedures before being released. The rain-gauged stations have a reasonably good spatial coverage and hence can be used to reveal the regional variability of extreme precipitation.

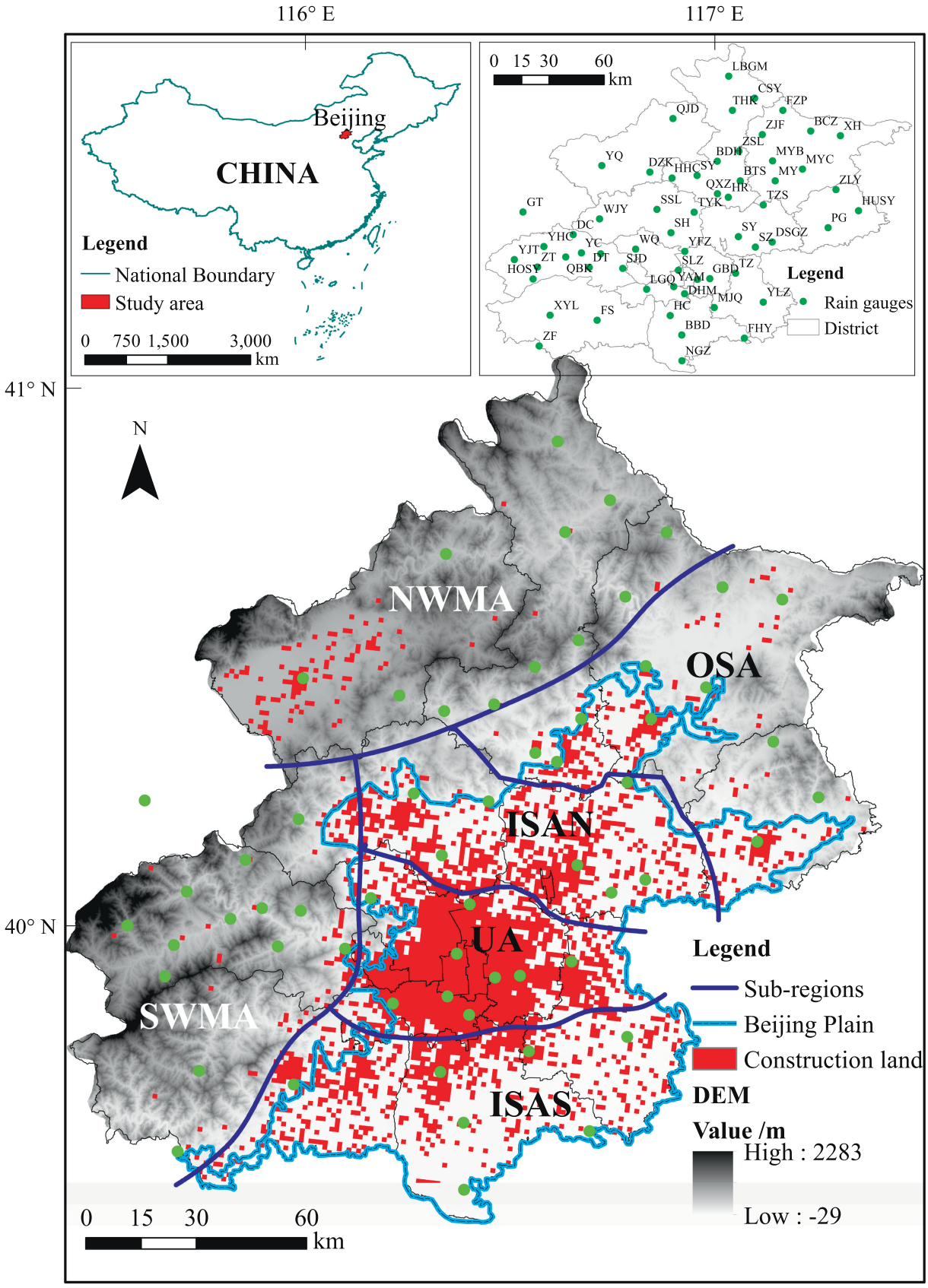

Fig. 1. The locations of the rain-gauge stations over the study area. The study area was divided into six sub-regions, including UA (urban area), ISAS (inner suburb area in the south), ISAN (inner suburb area in the north), OSA (outer suburb area), NWMA (northwestern mountain area), SWMA (southwestern mountain area). Red speckles represent the construction land areas in 2010 with the spatial resolution of 1km*1km.

2.1.3. Global climate indices

Several climate indices related to precipitation extremes are included in this study. In this work, the SOI (Southern Oscillation Index) and MEI (Multivariate ENSO Index) were used to discuss the ENSO (El Niño-Southern Oscillation) phenomenon. Generally, the negative values of SOI (known as El Niño episodes) are usually accompanied by a reduction in rainfall over eastern China (Fu et al., 2013), and positive values of the SOI (Tedeschi et al., 2016) are associated with wetter in eastern China than in normal year. The SOI indices during 1960–2012 were extracted from the Bureau of Meteorology of Australia (http://www.bom.gov.au/climate/current/soi2.shtml). The MEI indices during 1960–2012 were extracted from the National Oceanic and Atmospheric Administration (NOAA).

Another index used in this study is PDO (Pacific Decadal Oscillation), the leading principal component of monthly sea surface temperature anomalies in the North Pacific Ocean poleward of 20°N. The PDO is most frequently referred to as a long-lived ENSO-like pattern of Pacific climate variability, which might influence precipitation variation over China. The values of PDO index used here are also taken from NOAA covering a period of 1960–2012.

2.1.4. East Asian monsoon indices

While extreme precipitation events may well be teleconnected with pronounced ocean circulation anomalies, such as ENSO, it is worth investigating another closer link, the East Asian Monsoon (EAM). China is primarily affected by the EAM, which is divided into a warm and wet summer monsoon and a cold and dry winter monsoon (Ding, 1994). The EAM is characterized by strong northerly winds from the cold-core Siberia-Mongolia High in the winter and southerly winds with warm and moist air masses from the South China Sea and the Bay of Bengal in the summer. Several methods have been developed that aim to measure EAM intensity (Li and Zeng, 2002; Wang et al., 2008a; Wu et al., 2008). In this study, the East Asian summer monsoon index (EASMI) suggested by Li and Zeng (2002) was used. The dataset was downloaded from http://ljp.gcess.cn/dct/page/65577.

2.2. Methods

2.2.1. Extreme precipitation indices

Following Bonsal et al. (2001) and Wang et al. (2014), we define extreme precipitation events as those that exceed certain threshold percentiles of effective daily precipitation ($\geq$ 0.1 mm). In our analysis, three percentiles—90% (R90pT), 95% (R95pT), and 99% (R90pT)—were chosen as the thresholds for extreme daily precipitation analyses. A threshold is defined in terms of a fixed percentile of the daily rainfall amount series for each station, considering only days with non-zero rainfall, i.e., daily precipitation not $<$ 0.1 mm.

Additionally, the frequency and contribution ratios were also used to describe the number of days in which the daily rainfall amount exceeds a threshold and the ratio of the corresponding extreme precipitation to the annual total precipitation. Hence, in total, six extreme precipitation indices were used, i.e. frequency indices for three threshold values (R90pD, R95pD, and R99pD) and contribution ratios for three thresholds (R90pR, R95pR, and R99pR), as shown in Table 1.

2.2.2. Minimum cross entropy for change detection

In this study, we first evaluate changes in the distribution function of precipitation extremes (and indicators representing extremes discussed below) using the concept of minimum cross entropy (AghaKouchak, 2014; Singh, 2011). The principle of entropy is a powerful tool, widely used in different fields (Cui and Singh, 2017; Hao and Singh, 2012; Mishra et al., 2009; Sang et al., 2018). Minimum cross entropy is fundamental to information theory and is the basis for the Kullback–Leibler (KL) test (Kullback and Leibler, 1951) used to evaluate the divergence of two distributions from each other. Previous studies argue that the Kullback–Leibler test, also referred to as relative entropy, can be employed to detect changes in hydrologic time series (AghaKouchak, 2014). Here, the Kullback–Leibler test is used to measure changes in the statistics of extremes from 1981 to 2012 relative to the baseline of 1960–1980. The test reveals whether the distributions of precipitation extremes are different at a certain statistical significance level (here, $\alpha = 0.05$ significance level, representing 95% confidence).

Let's assume that the two different cumulative distribution functions of H and G represent the distribution functions of two extreme indicators (e.g., precipitation exceeding a certain threshold for two different periods). The Kullback-Leibler divergence (KL) can be expressed as:

$$KL(h,g) = E_h \log \frac{h(x)}{g(x)} \tag{1}$$

where, h and g, denote the density functions of H and G, respectively. H and G can be any indicator or data set with a distribution function. In Eq. 1, x is the indicator variable (in this study, precipitation extremes) and E_h represents the expectation over the density function h. Having discrete probability distribution functions described as $h = \{h_1, \ldots, h_n\}$ and $g = \{g_1, \ldots, g_n\}$, the Kullback-Leibler divergence can be expressed as:

$$KL(h,g) = \sum_{i}^{n} h_i \log \frac{h_i}{g_i} \tag{2}$$

where n denotes the sample size. Statistical hypothesis testing can be used to test the significance of the test. Here, the null hypothesis that the two distributions are statistically similar at $\alpha = 0.05$ significance level will be tested in 1981–2012 relative to 1961–1980.

2.2.3. Trends, correlations and heterogeneity analysis

The nonparametric Mann-Kendall test (Kendall, 1975; Mann, 1945) is also applied to identify the trend of all six indices. The main consideration of choosing the Mann-Kendall test is its non-parametric nature that assumes no particular underlying distributions (Ahmad et al., 2018; Pakalidou and Karacosta, 2018; Wang et al., 2017). A significance level $\alpha = 0.05$ was used in the test. The detailed information for the Mann-Kendall test is available in Mann (1945), Kendall (1975) and Song et al. (2014).

Table 1
List of the thresholds and extreme precipitation indices used in this study.

Acronym	Description	Unit
R90pT	Threshold value in the 90th percentile of daily precipitation series	mm
R95pT	Threshold value in the 95th percentile of daily precipitation series	mm
R99pT	Threshold value in the 99th percentile of daily precipitation series	mm
R90pD	Number of days with precipitation exceeding the threshold of the 90th percentile	days
R95pD	Number of days with precipitation exceeding the threshold of the 95th percentile	days
R99pD	Number of days with precipitation exceeding the threshold of the 99th percentile	days
R90pR	Ratio of extreme precipitation exceeding the 90th percentile to annual precipitation	–
R95pR	Ratio of extreme precipitation exceeding the 95th percentile to annual precipitation	–
R99pR	Ratio of extreme precipitation exceeding the 99th percentile to annual precipitation	–

The Pearson's correlation coefficient was used to explore the relationship between the extreme precipitation indices (variable X) and the climate indices (variable Y):

$$r = \frac{\sum (X - \overline{X})(Y - \overline{Y})}{\sqrt{\sum (X - \overline{X})^2 \sum (Y - \overline{Y})^2}} \quad (3)$$

where $\overline{X}$ and $\overline{Y}$ are the mean of X and Y, respectively. The statistical significance of the correlation coefficient was calculated using the Student's t-test (two-tailed test of the Student t distribution) at a significance level of $\alpha = 0.05$.

In order to reveal the geographical heterogeneity of the extreme precipitation indices, we followed Choi et al. (2014) and Ghosh et al. (2012) and calculated the spatial standard deviation and spatial skewness of extreme precipitation indices. To measure the deviation of the extreme precipitation index values from the mean across space, we calculated the standard deviation and skewness of each index across the area for each year. Higher values indicate a larger deviation across the area from the mean, and lower values indicate a smaller deviation. Positive skewness indicates that the data are spread out to the right of the mean and negative to the left. The skewness of a perfectly symmetric distribution is zero.

2.2.4. Wavelet transform coherence methods

Wavelet analysis allows one to determine dominant modes of variability and the change of those modes of time series. Traditional mathematical methods, such as Fourier transform, examine the periodicity of phenomena by assuming they are stationary in time. Wavelet analysis, however, decomposes time series into a time-frequency space and thus is able to extract localized intermittent periodicities. It is therefore particular useful in analyzing non-stationary time series. In this study, we make use of the wavelet transform coherence (WTC) method to analyze the coherence and phase lag between two time series as a function of both time and frequency (Grinsted et al., 2004; Jevrejeva et al., 2003; Soon et al., 2014).

Following Torrence and Webster (1999) for analysis of the covariance of two time series, the cross-wavelet spectrum of two time series X (e.g. extreme precipitation indices in this study) and Y (e.g. climate indices used in this study) with wavelet transforms W_X and W_Y as

$$W_{XY}(s,t) = W_X(s,t) W_Y^*(s,t) \quad (4)$$

where * denotes complex conjugation. And the cross-wavelet power is $|W_{XY}(s, t)|$. The phase angle of W_{XY} describes the phase relationship between X and Y in time-frequency space.

Additionally, the wavelet coherence is another measure of the intensity of the covariance of the two series in time-frequency space, which is defined as

$$R^2(s,t) = \frac{|S(f^{-1} W_{XY}(s,t))|^2}{S(f^{-1} W_X(s,t)) \cdot S(f^{-1} W_Y(s,t))} \quad (5)$$

where S is smoothing operator in both time and scale. The factor f^{-1} is used to convert to an energy density. The statistical significance level ($\alpha = 0.05$) of the wavelet coherence against back-ground red noise was estimated using Monte Carlo sampling. The detailed information about it can be referred to the work of Jevrejeva et al. (2003) and Torrence and Webster (1999). The MATLAB wavelet coherence package used here can be downloaded from http://www.glaciology.net/wavelet-coherence.

3. Results and discussion

3.1. Spatial pattern of extreme precipitation indices

For illustrative purposes, Fig. 2 portrays the spatial distribution of the chosen percentile values (the thresholds) and the annual total precipitation averaged over time. To better visualize the overall spatial pattern, the precipitation amounts and the thresholds from rain gauges were interpolated using the ordinary Kriging method. Fig. 2a shows a clear spatial trend for the total precipitation over Beijing with amounts increasing from the west to the east, and the largest amount appearing in the northeastern part of Beijing. Overall, the thresholds have a very similar spatial pattern, with a more apparent west-east variation pattern (Fig. 2b-d). They also vary from region to region, with the western mountainous areas having the lowest thresholds and the eastern plains area the largest. The R90pT, R95pT, and R99pT range from 18.2–29.4 mm (Fig. 2b), 25.8–43.8 mm (Fig. 2c), and 47.5–90.2 mm (Fig. 2d), respectively. According to the Chinese categorical classification of daily rainfall amounts (as shown in Table S1), R90pT rainfall events were found to be moderate (10–24.9 mm/day), except for the northeastern and southwestern areas. On the other hand, the R95pT and R99pT rainfall events are classified as “heavy rain”, and “rainstorm”, respectively.

For the same thresholds, the spatial patterns of the frequency of extreme precipitation and their contribution ratios are presented in Fig. 3 after interpolation using the same technique. Overall, the spatial patterns of frequency are similar to that of total precipitation and the extreme thresholds, indicating more extreme events in the northeastern part. However, the spatial distributions of the frequency (e.g., R90pD, R95pD, and R99pD) do not necessarily match those of the high thresholds shown in Fig. 2. For example, the lowest value of R90pD is in the southeastern part of Beijing, not in the western mountainous area, as commonly believed. The highest value of R99pD is in the southwestern region near the Zhangfang station and in the northeastern region near the Xiahui station (Fig. 3c). Fig. 3 also provides the spatial pattern of the contribution ratio of extreme precipitation to the annual total precipitation amount. We found that the highest values of R90pR and R95pR are in the edge zones between the mountainous area and the plains area with zonal distribution (Fig. 3d-e). The largest value of R99pR occurs at the Fangshan and Zhangfang stations in the Fangshan district, which is known to have a high risk of flooding (Zhang et al., 2013). This indicates that one extreme event (Thiombiano et al., 2017) can contribute to 13%–14% of the annual total precipitation (see Fig. 3f) and lead to high flood risk.

3.2. Temporal trend of extreme precipitation indices

Time series of extreme precipitation indices (Fig. 4) indicate that temporal variations of extreme precipitation in Beijing had both inter-annual and inter-decadal variability. The changes in the frequency indices (R90pD, R95pD and R99pD) during 1960–2012 are showed in Fig. 4a, Fig. 4b and Fig. 4c, respectively. The results show that the R90pD varies from a low of 2.7 days in 1980 to a high of 9.5 days in 1969, with a mean of 5.9 days. Similarly, the R95pD ranges from 1 day (1980) to 5.4 days (1969) with a mean of 3 days, and the R99pD ranges from 0.1 day to 1.5 days with a mean of 0.6 day during the 1960–2012 period. For the contribution ratio indices (Fig. 4d-f), the highest values of precipitation extremes were 66.50% and 51.04% in 1994 for R90pR and R95pR and 29.41% in 1963 for R99pR, respectively. The lowest values were 26.57% and 13.30% in 1980 for R90pR and R95pR, and 1.23% in 2010 for R99pR, respectively. The five-year moving-average curves for extreme precipitation indices emphasize the inter-annual and inter-decadal variability and the time series of these six indices show diverse temporal variations, as displayed in Fig. 4. Note that higher-percentile indices often have larger variations. In addition, the signature of several major climate conditions, including severe droughts, is evident in the time series. For example, during the 12-year drought from 1999 to 2010 there were remarkably fewer extreme rainfall events. In contrast, 2012 was a wet year and the results show a high frequency and contribution rate for extreme thresholds. The inter-annual variability of precipitation extreme indices is somewhat similar to that of the annual precipitation reported in Song et al. (2014).

Fig. 4 also shows that all six indices exhibit a decreasing trend

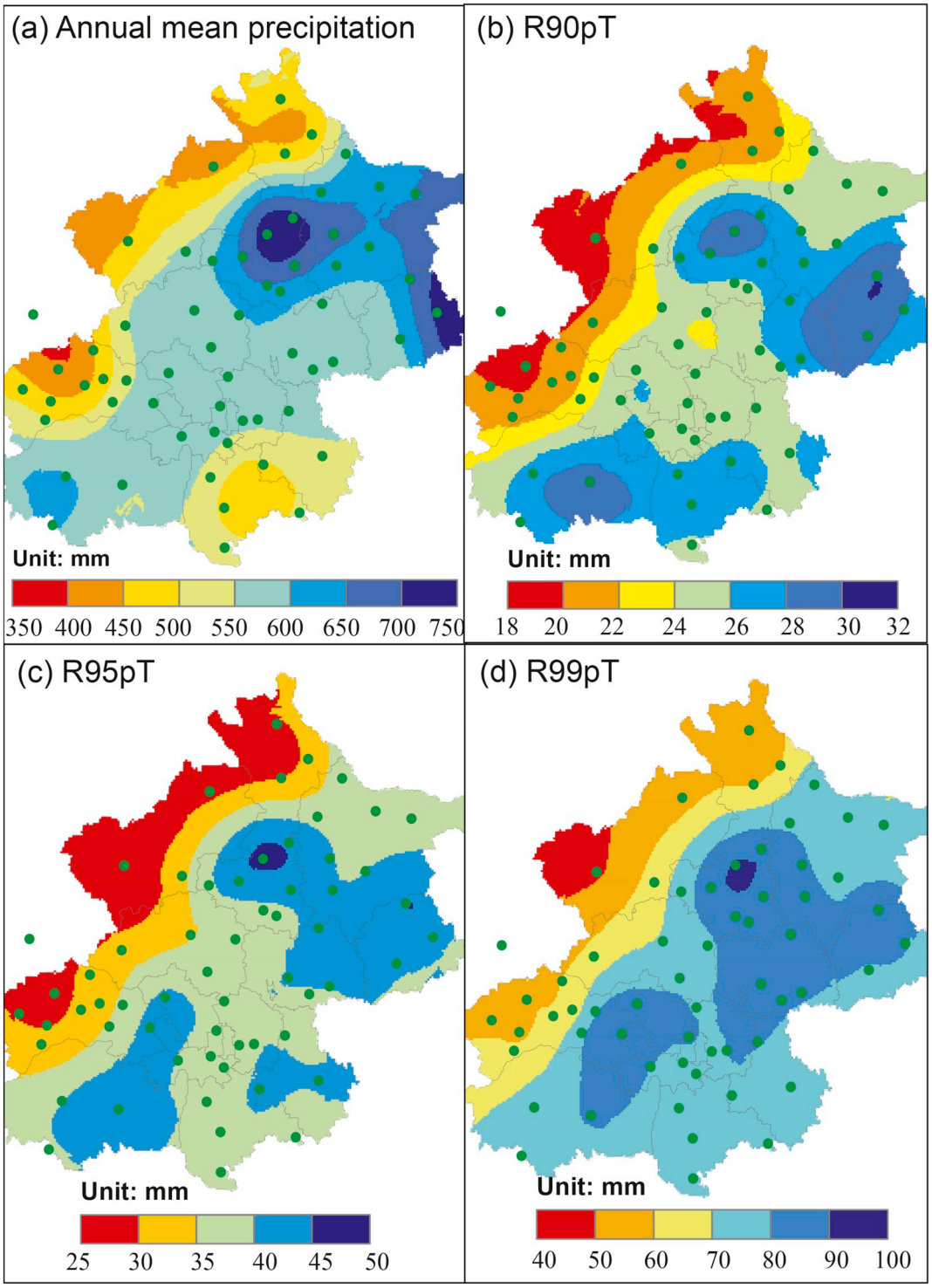

Fig. 2. The spatial distribution of annual mean precipitation (a) and extreme precipitation thresholds in Beijing during 1960–2012 at: (b) the 90th percentile, (c) the 95th percentile, and (d) the 99th percentile, respectively.

during the last 50 years. The regional R90pD and R95pD indices show a stronger decreasing trend of −0.15 day per decade in the 1960–2012 period, while R99pD has a slope of −0.07 day per decade during the same period. For the contribution ratio indices, the decline magnitudes are 2%, 2%, and 1% per decade for R90pR, R95pR and R99pR, respectively. Overall, the declining trend of all six indices becomes stronger when the threshold percentiles vary from the 90th percentile to the 99th percentile. Feng et al. (2007) and Fu et al. (2013) showed that the 1960s were the wettest period for northern China, resulting in a general decreasing trend and serious water crisis in the region. Additionally, the Mann-Kendall test was also used to detect the trend of all the six indices, as shown in Fig. 5. Overall, all the six indices showed a negative trend since 1980s, especially during the second half of the 2000s, with a statistically significant trend at a level of $\alpha = 0.05$. From Fig. 5, we can also detect an abrupt point for these indices. The changing point occurs in the middle and late-1990s for the frequency indices, while it appears in 1980 for the contribution ratio indices, except for R99pR which has more than one change point.

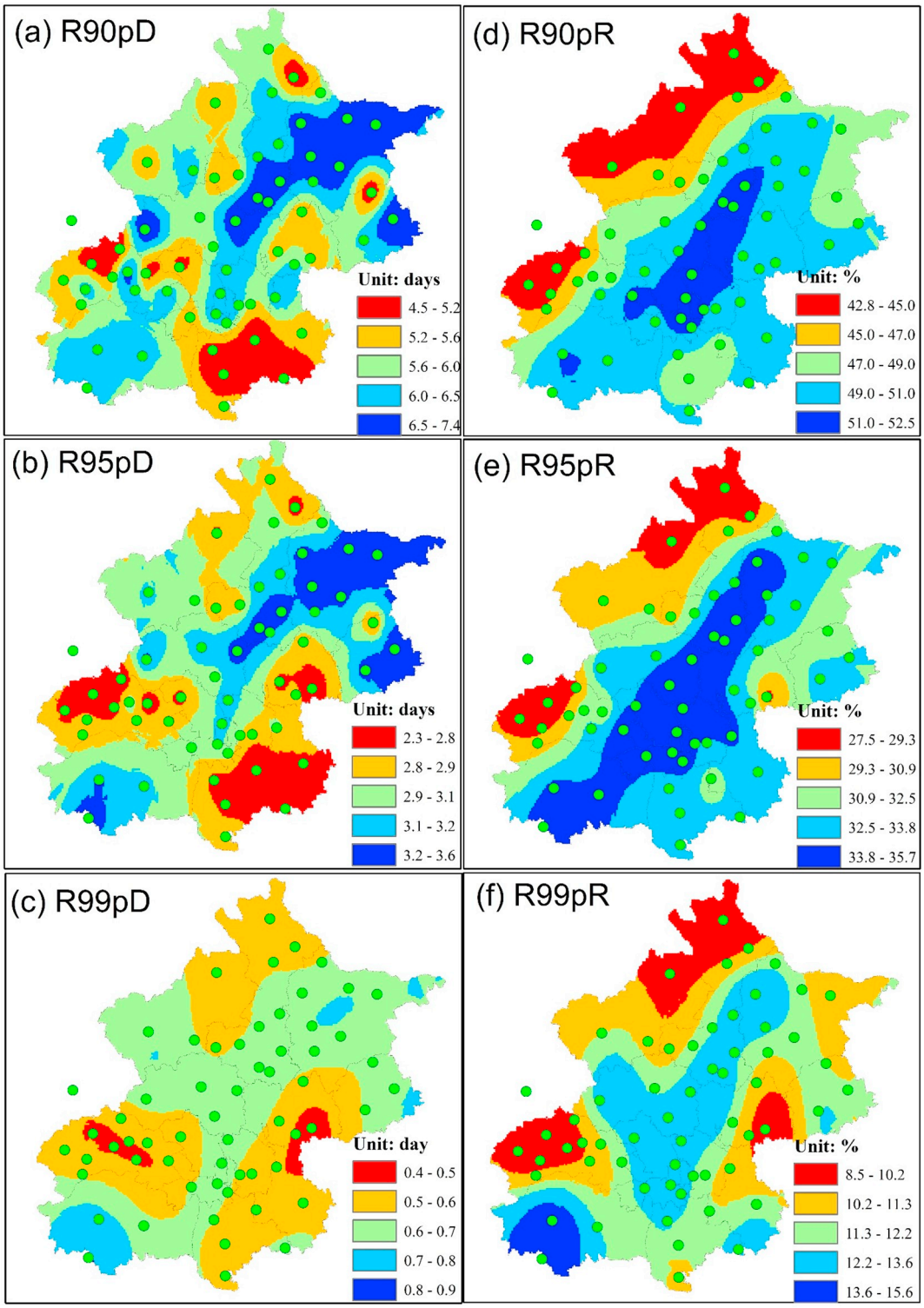

Fig. 3. The spatial variation of the frequency (R90pD, R95pD and R99pD) and contribution ratio (R90pR, R95pR and R99pR) of extreme precipitation at the different threshold percentiles (the 90th, 95th and 99th percentiles).

The results of the Mann-Kendall test for each station are shown in Fig. 6. For R90pD, most stations (50) do not show any significant trends. Trends are significant for 10 stations at the 95% confidence level (Fig. 6a). While for R90pR, there are 10 stations with a statistically significant decreasing trend and 7 stations with a statistically significant increasing trend at the $\alpha = 0.05$ level (Fig. 6d). Regarding to the R95pD (Fig. 6b) and R95pR (Fig. 6e), there are nine and eight stations with a statistically significant positive trend, respectively. For the same indices, 5 and 11 stations show a statistically significant negative trend. From Fig. 6c and f, we can see that only one station shows a significant decline trend for the R99pD. For R99pR, one station shows a significant increasing trend and three stations show a statistically significant decreasing trend. Overall, increasing trends for the extreme precipitation indices mostly occurred in urban areas and the southern part of the Beijing plain area.

In order to detect whether the extreme precipitation indices show

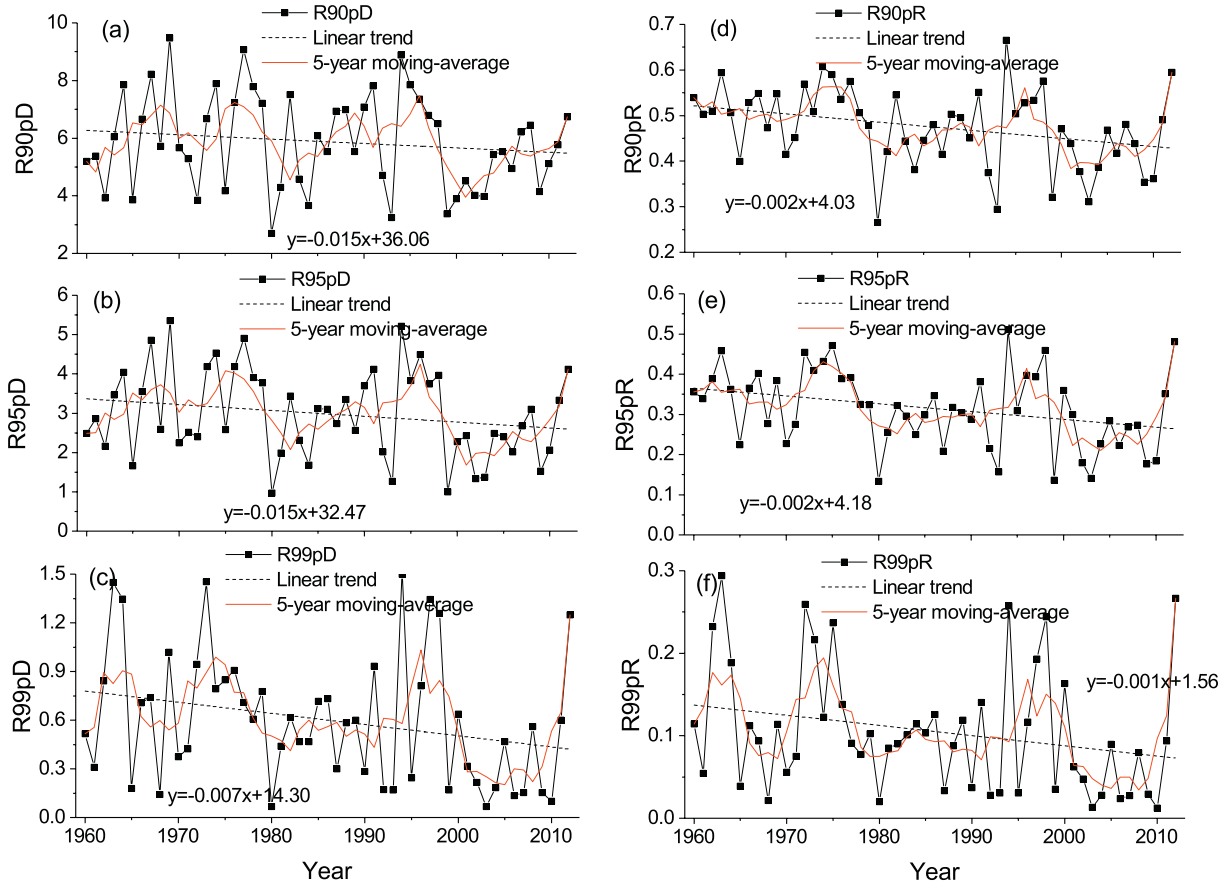

Fig. 4. Time series for each extreme precipitation index in Beijing during 1960–2012.

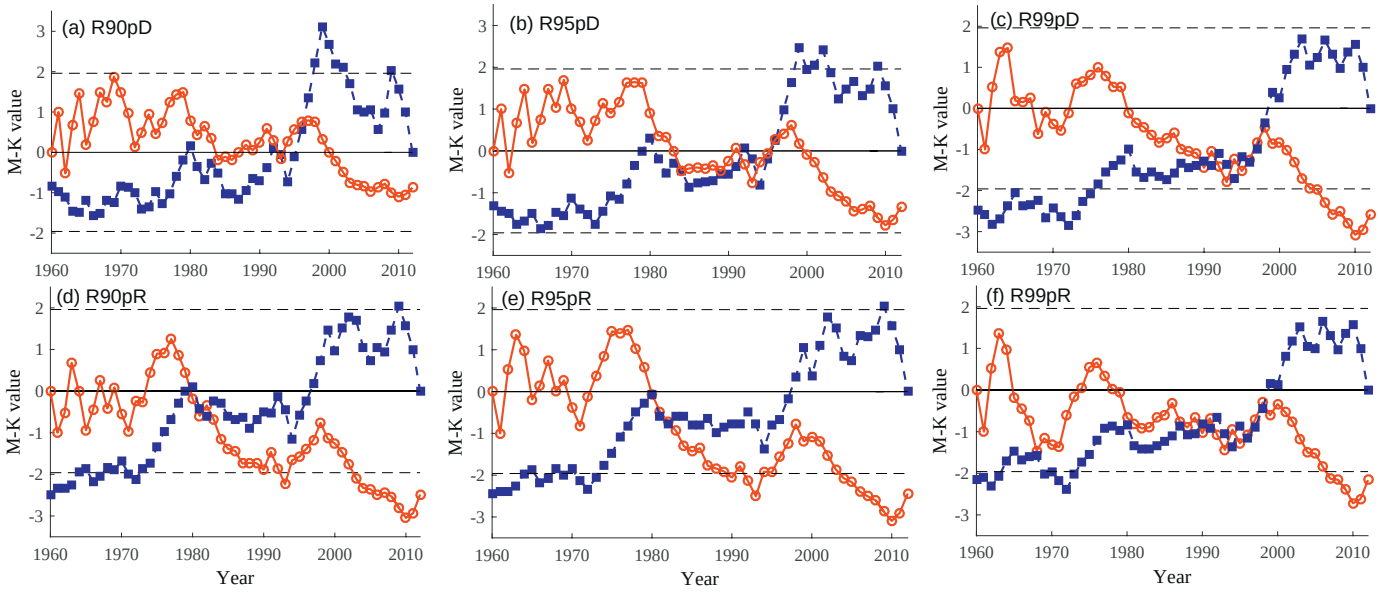

Fig. 5. The time series of the Mann-Kendall trend test for all extreme precipitation indices.

significant change between the different periods (1960–1980 and 1981–2012), we also perform change detection analysis using the entropy-based approach explained in Section 2.2.2. Fig. 7 shows the Kullback-Leibler (KL) divergence test results for extreme precipitation indices for each station during the two periods (1960–1980 and 1981–2012). The results show that most of the stations (46 stations, 76.67%) for the R90pD and the R95pD, 31 (51.67%) for the R99pD, 48 (80%) for the R90pR, 50 (83.33%) for the R95pR and the R99pR) show a significant change at $\alpha = 0.05$ significance level in 1981–2012 relative to 1960–1980. For the frequency indices, almost half of the stations (e.g. 31, 34 and 27 for the R90pD, R95pD and R99pD, respectively) show a significantly decreasing trend between the two periods (Fig. 7a-c), while the percentage of the ones that exhibit statistically significant increase falls from 25% (15 stations) for the R90pD (Fig. 7a)

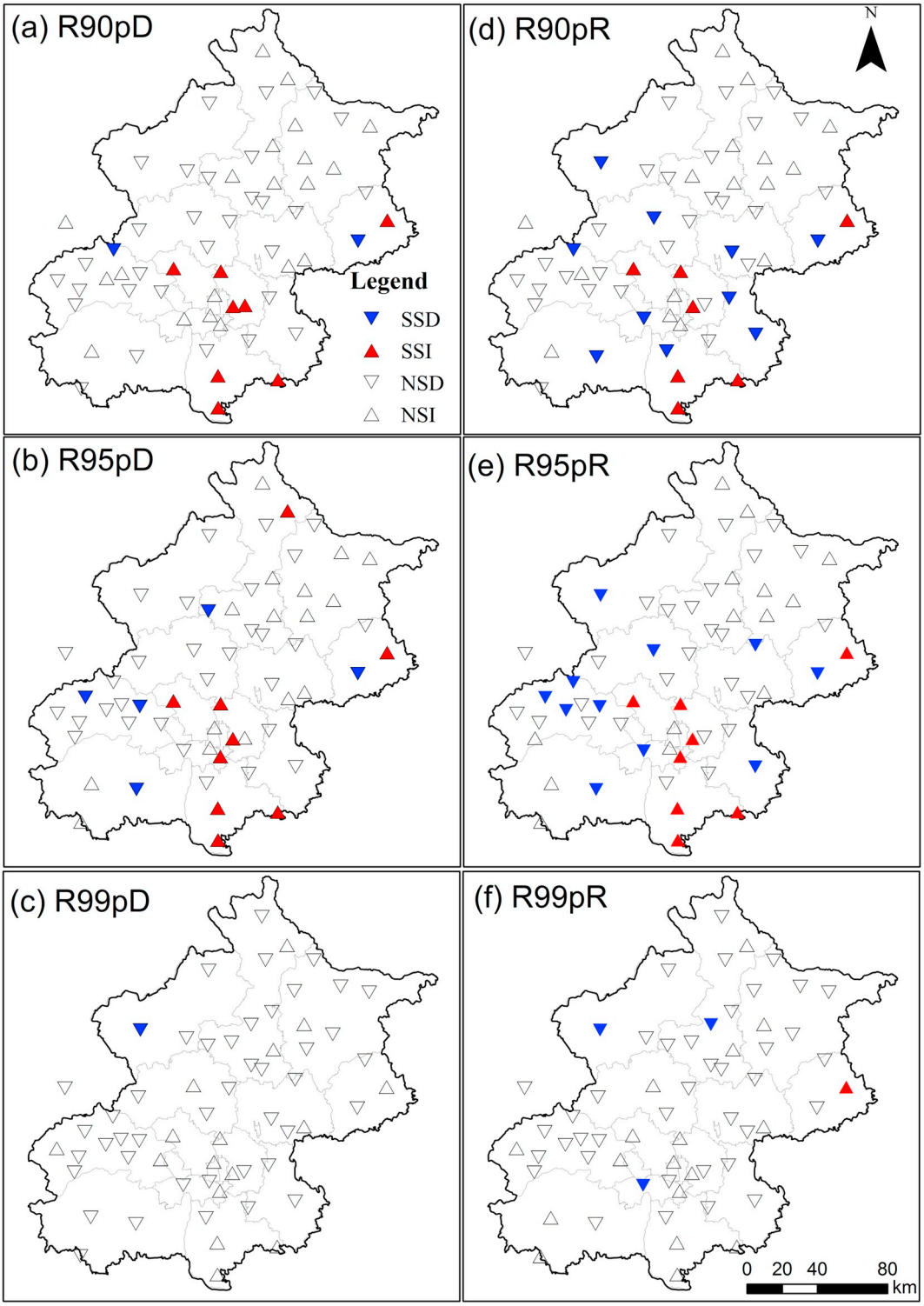

Fig. 6. Spatial distribution of annual trends of (a) R90pD, (b) R95pD, (c) R99pD, (d) R90pR, (e) R95pR, (f) R99pR. Filled red triangle denotes significant increase at a level of $\alpha = 0.05$, inverted filled blue triangle denotes significant decrease, open triangle denotes no significant change. SSD means statistically significant decreasing. SSI means statistically significant increasing. NSD represents non-significant decreasing, and NSI is non-significant increasing.

to 5% (3 stations) for the R99pD (Fig. 7c). This indicates that 25% of the stations show the precipitation extremes based on R90pD have increased, while only 5% exhibit a similar behavior for R99pD. Similar results are provided for the contribution ratio indices (Fig. 7d-f). As shown for contribution indices, a decreasing trend has been observed in most stations, especially for higher thresholds.

Fig. 8 shows the mean values of the six extreme precipitation indices for each station during the two periods (1960–1980 and 1981–2012). For 60 stations (the detailed information can be seen in Table S2), the rate of change in the frequency indices is −3.2%, −8.6% and − 19.8% for the R90pD, R95pD and R99pD, and − 7.32%, −12.67% and − 22.42% for the three contribution indices (e.g. R90pR, R95pR and R99pR), respectively. That is to say, the frequency and contribution indices show a decreasing trend, similar to the above gradual change in

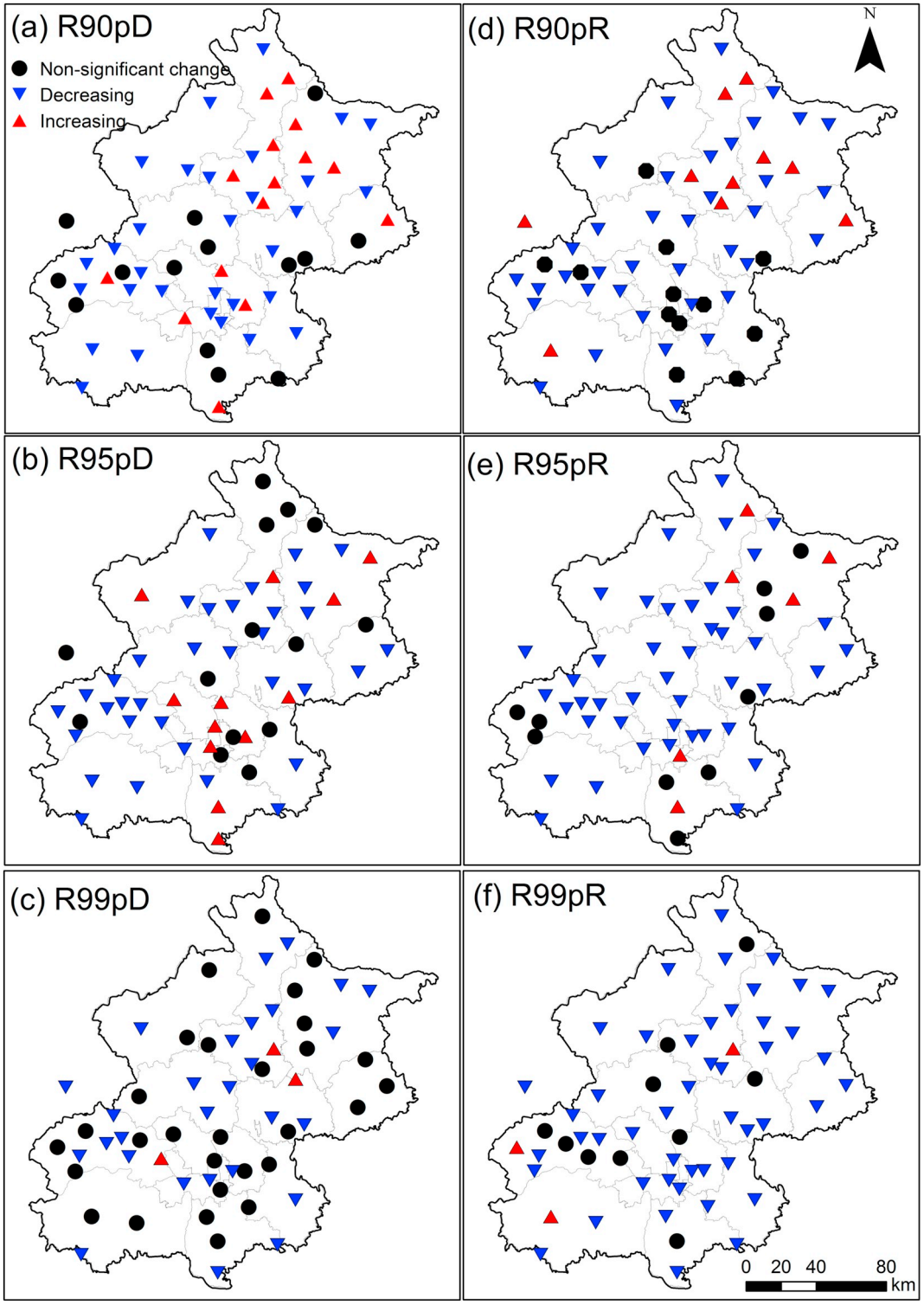

Fig. 7. Statistically significant change of the extreme precipitation indices at 95% confidence in 1981-2012 relative to the baseline period of 1960-1980 using the principles of entropy. Black circle represents non-significant change during the two periods. Blue triangle means decreasing trend and red triangle is increasing trend.

the six indices. In view of these results, we found some stations that exhibit insignificant change based on the KL test, yet they seem to have high rates of change in the extreme precipitation indices in 1981–2012 relative to 1960–1980. This indicates that in some stations, the extremes have changed, but the overall distribution function has not changed significantly. Overall, the results of the KL test are consistent with the MK trend test analysis results.

3.3. Changes in the spatial variability of extreme precipitation indices

Temporal changes of each extreme precipitation indices for each station during 1960–2012 are illustrated in Fig. 9. The extreme precipitation events usually occur at the same time of the year for a large portion of the stations considered in this study, implying high spatial correlation patterns of extreme precipitation events. Generally speaking, the high occurrences of frequency of precipitation extremes

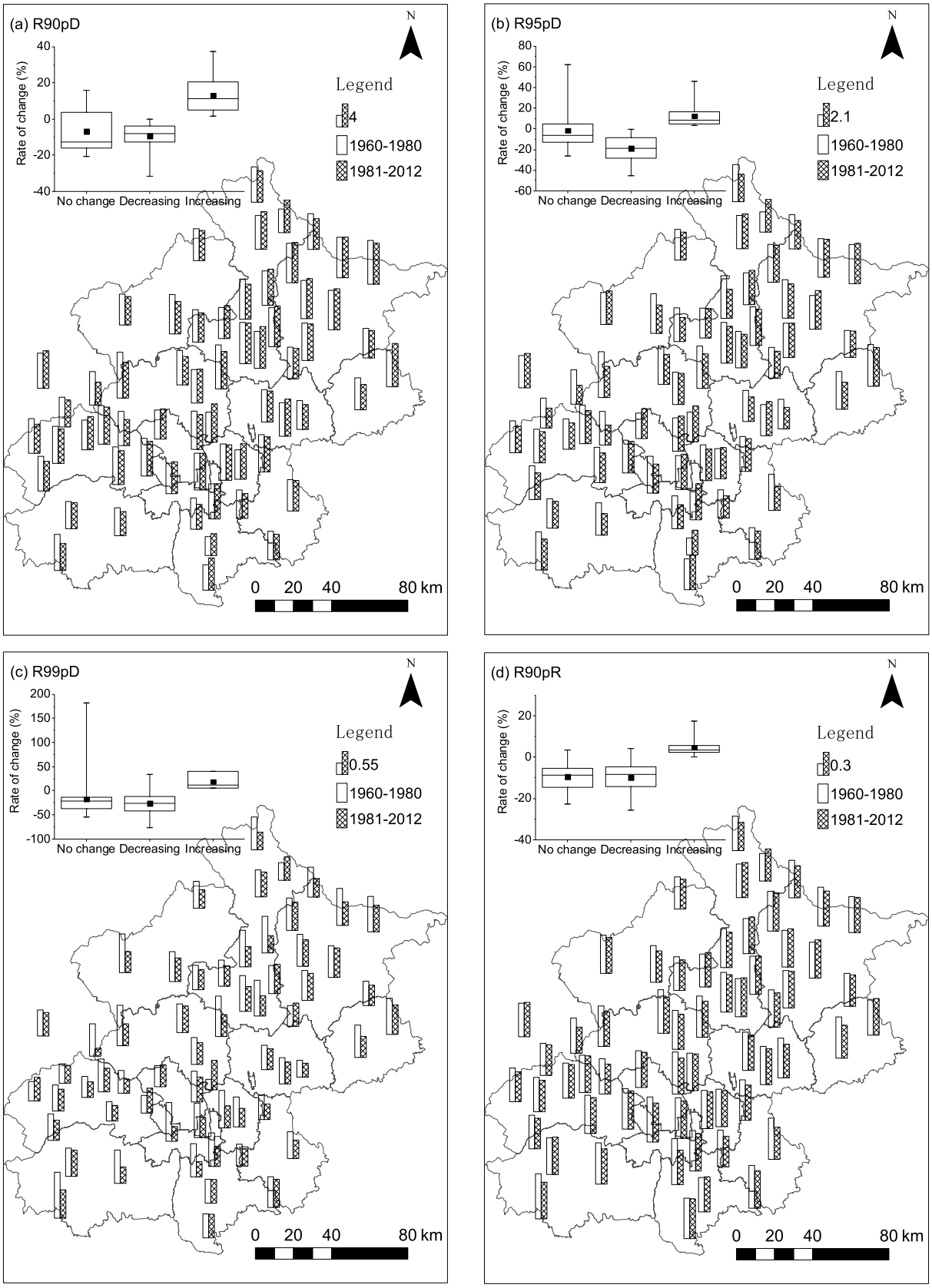

Fig. 8. The mean of the extreme precipitation indices for each station between the periods of 1960-1980 and 1981-2012. The hollow box represents the mean value of precipitation extremes in the period of 1960-1980, and the filled box represents the mean value in 1981-2012. The length of box represents the magnitude of mean values. The box-plot shows the ratio of changes during the two periods, with the mean ratio marked black squares. The source data can be seen in Table S2

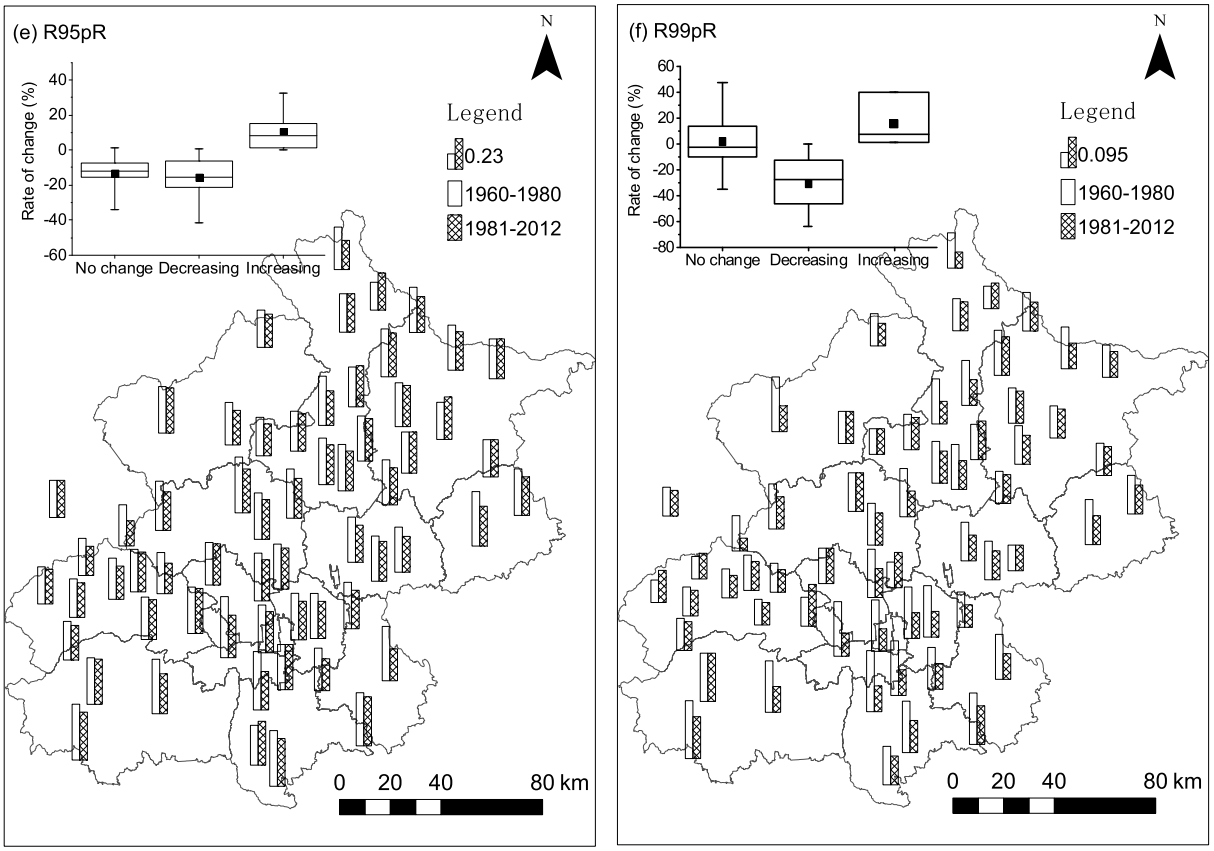

Fig. 8. (*continued*)

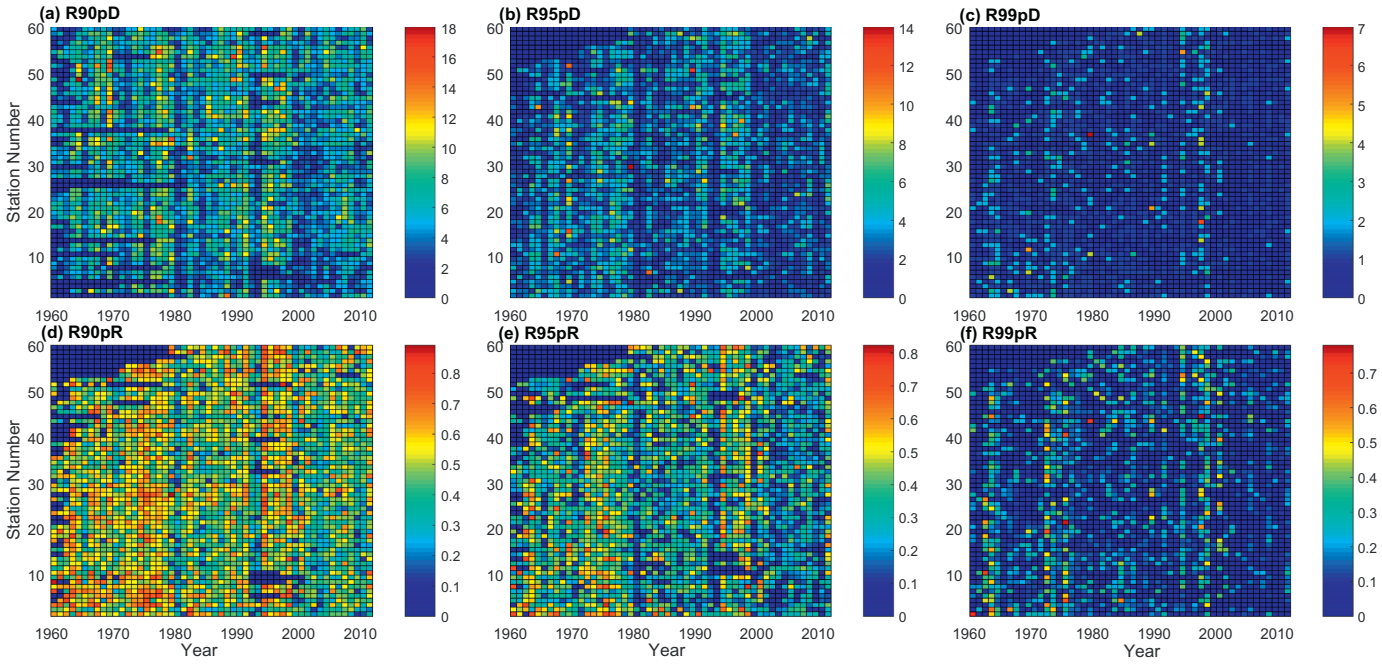

Fig. 9. Changes of extreme precipitation indices for all rain-gauge stations during 1960–2012.

(R90pD, R95pD, and R99pD) are observed mainly in the late-1960s, late-1970s, and mid-1990s (Fig. 9a-c). A similar feature is observed for the contribution ratio indices, i.e., R90pR and R95pR (Fig. 9d-e). For R99pR, the high values occur in the early-1960s, mid-1970s, and late-1990s, approximately (Fig. 9f). In summary, conspicuous spatial dependence of precipitation extremes implies higher probability of simultaneous occurrences of heavy precipitation regimes across the entire Beijing area, thereby exposing the region to flood hazards.

Fig. 10 shows the geographical heterogeneity of the indices in terms of their spatial distribution of standard deviation and spatial skewness. The frequency indices of extreme precipitation commonly have high values in the late-1960s, late-1970s, and mid-1990s. Except for R90pD,

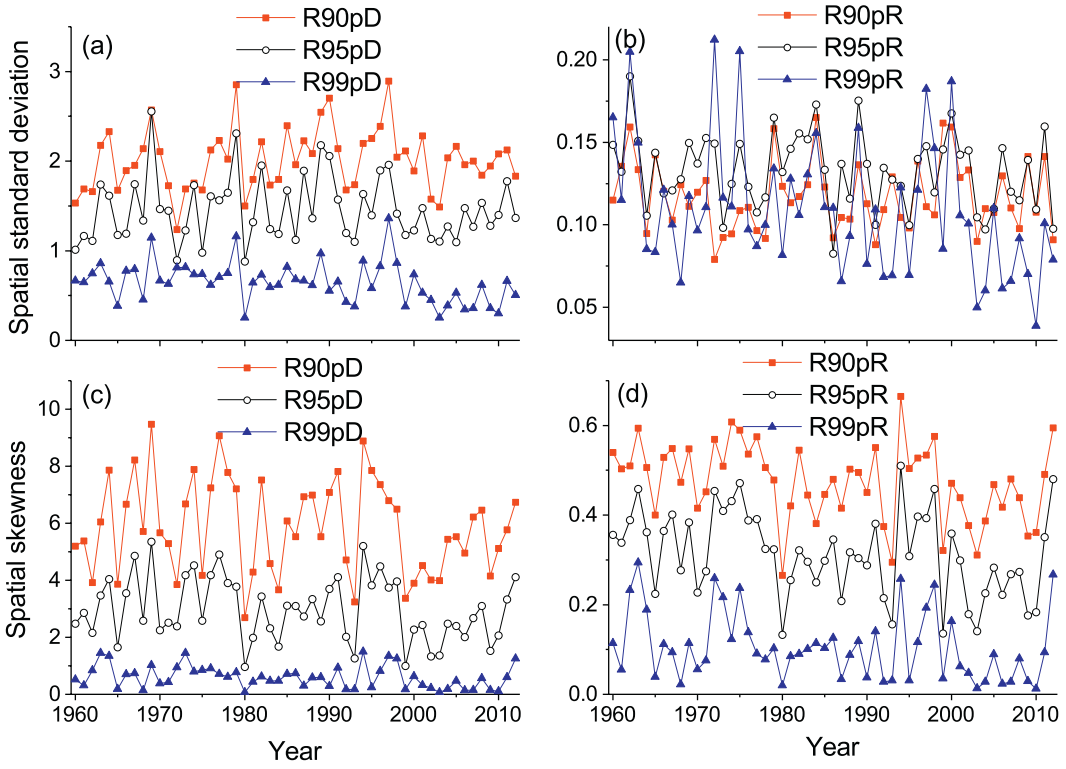

Fig. 10. Spatial standard deviation and spatial skewness of extreme precipitation indices for each year (1960–2012).

geographical heterogeneity of extreme precipitation indices shows a slight decreasing trend (Fig. 10b-c, Fig. 10g-i). Additionally, higher spatial variability of the frequency indices also occurs in the late-1960s, late-1970s, and mid- and late-1990s. Similar results are also observed for the contribution ratio indices. Fig. 10 also portrays the skewness for each year. Positive skewness is dominant except for R90pR and R95pR, indicating that histograms will be stretched to the right. Negative skewness is dominant for R90pR with the histogram stretching to the left. R95pR shows some fluctuation between positive and negative within a small range, indicating a near symmetric distribution around the mean.

Fig. 11 shows scatterplots between the spatial standard deviation and the spatially averaged indices. All three frequency indices show a positive correlation, suggesting that geographical heterogeneity tends to increase with the indices. For the contribution ratios, similar results are also shown for R99pR. However, R90pR and R95pR reveal a negative correlation, as shown in Fig. 11b. The positive correlation coefficient between the spatially averaged value and spatial standard deviation implies positive skewness of extreme precipitation indices (Figs. 9 and 10). Similarly, the negative correlation coefficient represents negative skewness for precipitation extremes.

3.4. Possible causes to changes of extreme precipitation

The changes of the total and extreme precipitation over China are very complicated, with many influence factors or drivers, such as the East Asian monsoon, global climatic indices (i.e., ENSO, PDO, IOD, NAO, etc.), global climate change, etc. However, a thorough and comprehensive discussion of this issue is beyond the scope of this study. Instead, the influences of ENSO, PDO, East Asian monsoon, urban heat

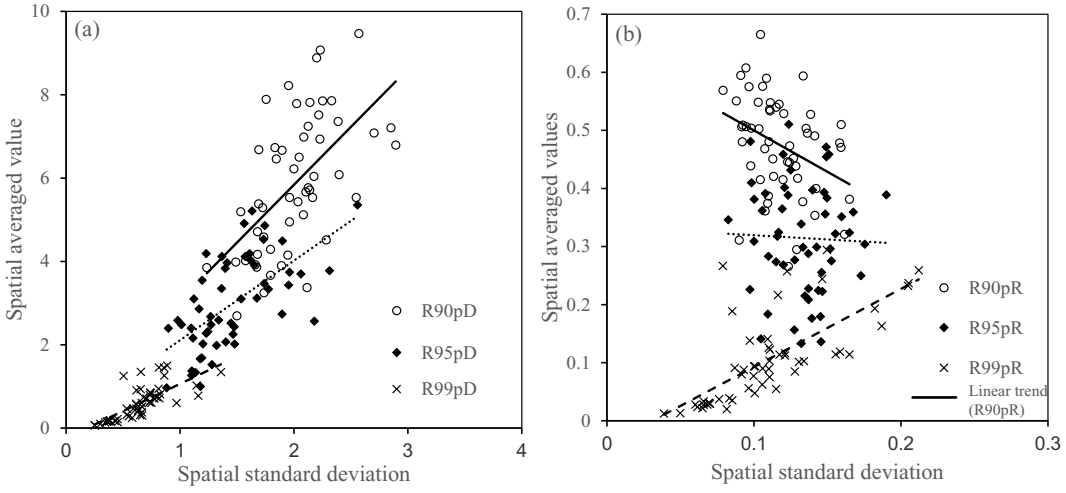

Fig. 11. Scatterplot between the spatially averaged value of extreme precipitation indices and spatial standard deviation for the extreme precipitation indices.

island and topography on the extreme precipitation over Beijing area are briefly discussed as follows.

3.4.1. ENSO and PDO

ENSO significantly influences extreme precipitation at local and regional scales in some parts of the world (Kenyon and Hegerl, 2010; Min et al., 2011). However, the influence of ENSO on extreme precipitation can be positive in some areas and negative in other areas, or the reverse, depending upon the phase of the ENSO cycle. The influence of ENSO on extreme precipitation in China has been well studied (Fu et al., 2013; Li et al., 2011; Niu et al., 2014; Wang et al., 2012; Wei et al., 2014; Ye, 2014; Zhang et al., 2014). For example, Li et al. (2011) found that during winter and spring, extreme precipitation events occur more often during El Niño events than during La Niña events. During summer and autumn, the opposite is true. Shen (2012) and Wang (2011) discussed the effect of the ENSO on the extreme precipitation events in northern China. They found that precipitation decreases in a stronger La Niña year, but it increases when El Niño or a weak La Niña occurs. Fu et al. (2013) found that the extreme precipitation of northern China has a teleconnection with SOI at interdecadal scale but is only statistically significant during certain times. Additionally, the relationship between the PDO and precipitation in China has also been well studied. For example, Chen et al. (2013) concluded that above-normal precipitation tends to occur more in northern China during the negative PDO phases, while above-normal precipitation occurs in central China during the positive PDO phases. Chan and Zhou (2005) found that the interdecadal variation in summer precipitation over south China coincides more with dry monsoon years during the periods of high PDO index, and vice versa. Ouyang et al. (2014) revealed that precipitation decreased overall during El Niño/PDO warm phase periods and increased during La Niña/PDO cool phase periods in most of China. Zhao et al. (2014b) found consistency in the periodic variation of extreme precipitation in Pearl river basin and that of the PDO.

As already noted, the indices of ENSO (measured by the SOI and MEI) and PDO considered in this study are the annual average values and the annual time series of the SOI, MEI, and PDO are illustrated in Fig. S1. It appears that the SOI shows a decreasing trend while the MEI and PDO show an increasing trend. The PDO experienced an obvious shift from a cool phase to a warm phase around 1976; while the minimum SOI and maximum MEI occurred at around 1987. The relative higher MEI or lower SOI occurred around 1983, 1992, 1997. As mentioned in Section 3.2, the change-point for extreme precipitation indices appeared around the beginning of 1980s and the end of 1990s. To some extent, the change point of extreme precipitation may be influenced by the ENSO In this study, we also considered a link between the observed extreme precipitation modes of variability and the possible influence of well-established climate indices. Table 2 shows the Pearson correlation coefficients between the annual precipitation, extreme precipitation indices and climate indices. There is a negative correlation between annual precipitation and the three climate indices, though not a statistically significant one. Except for the R95pD, the SOI and MEI exist as different phases of the correlation coefficients with the extreme precipitation indices. For the PDO, a negative correlation was found for all the extreme precipitation indices, but is only statistically significant for the contribution indices of extreme precipitation. Additionally, we explore the coherence of the leading extreme precipitation indices with ENSO and PDO through the cross wavelet spectra as shown in Fig. 12. This indicates that the inter-decadal teleconnection between climate indices and extreme precipitation indices is statistically significant at certain time periods. For example, a statistically significant relationship exists between the R90pD (R95pD) and the PDO at an 8- to 10- year period scale, whereas the R99pD and the PDO have a significant relationship at a 5- to 6- year period scale. For the contribution indices and the PDO a significant relationship exists at a 1- to 2- year period scale. Overall, significant relationships occurred during the end of the 1990s. However, Fig. 12 also shows that relationships between the ENSO (SOI and MEI) and the extreme precipitation indices at the 90th and 95th percentile do not have statistical significance, except for R99pD and R99pR within a certain time period.

3.4.2. The East Asian Monsoon

The influence of the East Asian monsoon on precipitation regimes over China has been well studied. For example, Wang and Zhou (2005) have shown a strengthening trend of the Eurasian continental high and a weakening trend of the western Pacific subtropical high, thus limiting the northward extension of the summer monsoon in the central-east China and causing a longer Meiyun season in the Yangtze river basin as well as a shorter rainy season in North China. As a result, they concluded that the annual and summer mean precipitation and the extreme precipitation events consistently decreased. Similar conclusions are also obtained by other researchers (Ding, 2007; Ding and He, 2006; Ding et al., 2007; Ding et al., 2009; Ding et al., 2008; He et al., 2006; Liu and Ding, 2008; Liu et al., 2014; Ren et al., 2012; Xu et al., 2006; You et al., 2011; Zhou et al., 2010), which agrees well with the results on the frequency of extreme precipitation in this study. Fig. S1 shows a decreasing trend for the annual mean EASMI from 1950 to 2012. Overall, the EASMI shows a decreasing trend during this period. We analyzed the relationship between precipitation indices and EASMI and the results are also shown in Table 2. Only the annual precipitation and the R90pD show negative correlations with the EASMI, although the correlations are not statistically significant. The other two frequency indices show a positive correlation with the EASMI. Significantly positive correlations were found between the EASMI and all the contribution indices of extreme precipitation. From Fig. 12, we can conclude that there is a significant relationship between the EASMI and the extreme precipitation indices during the end of 1970s and the 1980s, except for the R99pD and R99pR. To some extent, the decreasing trend of EASMI since the end of 1970s has significantly influenced extreme precipitation over Beijing, especially for the contribution indices at the 90th and 95th percentile.

3.4.3. Urban expansion and UHI

Since China implemented the reform and open policy and began the transition from a centrally-planned, rural-based economy to a market-oriented, urban-based economy in 1978, Beijing has experienced fast economic development and unprecedented urbanization (Wu et al., 2015; Zhang et al., 2016). Urban expansion is known to affect precipitation. To emphasize the important role of urbanization in extreme precipitation, we address the differences in the change of extreme precipitation indices for the urban and suburb areas in Beijing. According to the work by Song et al. (2014), the suburb areas include the inner suburb and the outer suburb areas in Beijing. However, there are reversed differences in precipitation amounts between the outer suburb and urban area due to the impact of terrain in Beijing's case. Thus, in this study, we primarily focus on the differences in precipitation extremes between the inner suburb and the urban areas to analyze the effect of urban expansion on the distribution of precipitation extremes. Similar to Song et al. (2014), the inner suburb area was divided into two parts, i.e. the inner suburb area in the north (ISAN) and in the south (ISAS). There are 21 stations located in the inner suburb and the urban areas, as shown in Fig. 1 and Table S3, including 9 stations (WQ, YFZ, SLZ, LJHY, GBD, YAM, DHM, LGQ, TZ) in the urban area (UA), 6 stations (SH, SY, SZ, DSGZ, SSL, TYK) in the ISAN, and 6 stations (HC, MJQ, YLZ, BBD, FHY, NGZ) in the ISAS. The ISA includes the ISAN and ISAS. We estimate the extreme precipitation indices for the four subregions to assess the change in the precipitation extremes, and then compare the changes of extreme precipitation indices in the urban area with that of the suburb area, as shown in Table 3 and Fig. 13. Overall, most of extreme precipitation indices in the UA are slightly larger than that in the ISA/ISAN/ISAS for these three different time series. For the second period (1981–2012), the ratios of frequency indices (e.g. the R90pD and R95pD) in the UA to that in the ISA have less of an increase

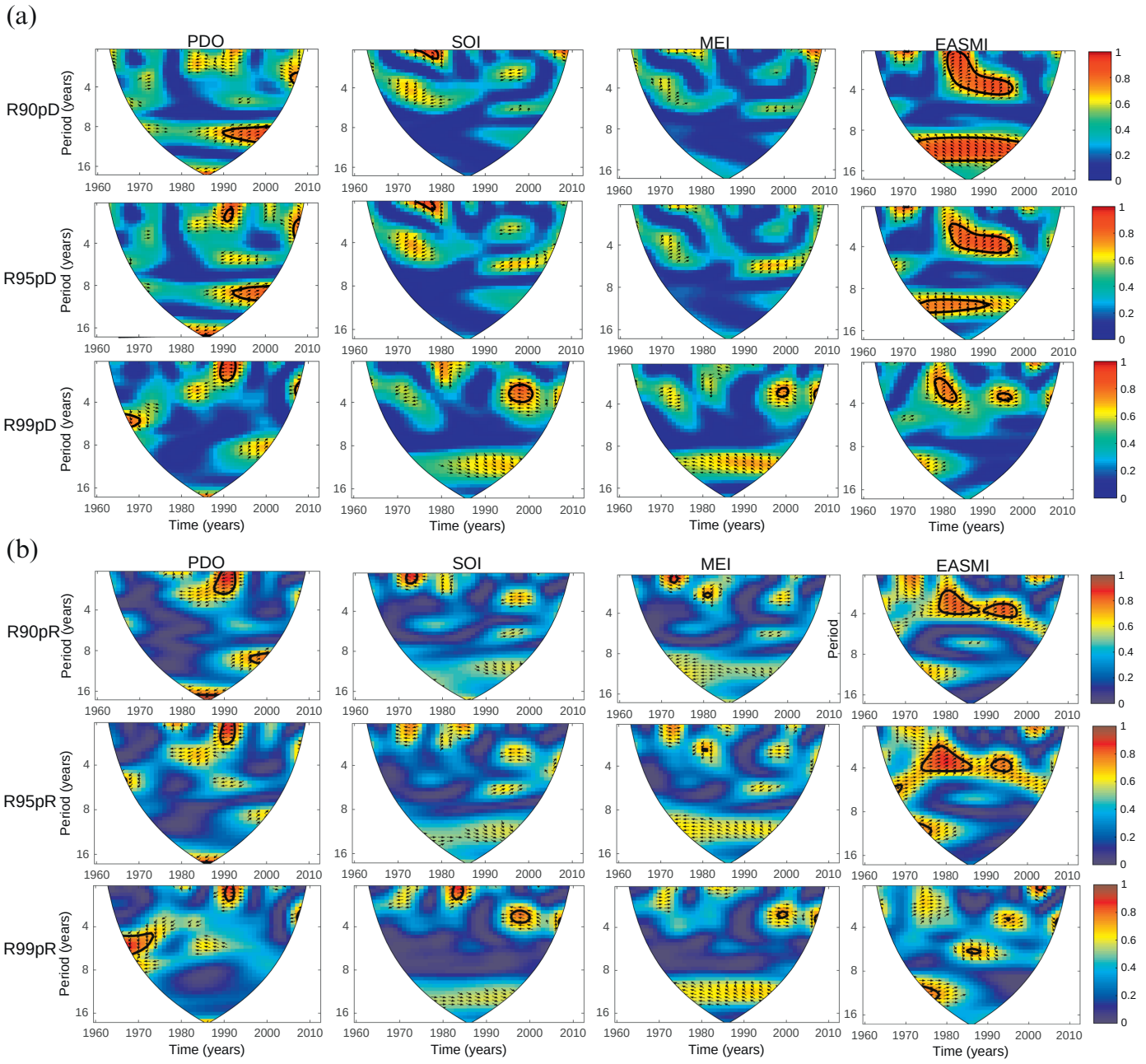

Fig. 12. Wavelet squared coherence between the standardized extreme precipitation indices and the climate indices during the period of 1960-2012. The thick black line is the 5% significance level using the red noise model and the thin black line indicates the cone of influence. Phase arrows indicate the relative phase relationship between the extreme precipitation indices and climate indices series, point right (in-phase), pointing left (anti-phase), pointing down (extreme precipitation indices leading climate indices by 90°), and pointing up (climate indices leading extreme precipitation indices by 90°)

compared with the first period (Gao and Xie, 2016). While the ratio of R99pD in the UA to that in the ISA has an opposite change, changing from 1.10 to 1.06. However, for the contribution ratio indices, there are different change patterns for the three thresholds. The ratio of R90pR in the UA to that in the ISA increases by 4% from the first period to the second period, while the ratios for the other two thresholds have a slight decrease with a decline rate of 9% and 15%.

Table 2
Pearson correlation coefficient between the precipitation indices and the climate indices.

	Annual precipitation	R90pD	R95pD	R99pD	R90pR	R95pR	R99pR
PDO	−0.111	−0.029	−0.133	−0.216	**−0.307***	**−0.326***	**−0.303***
SOI	−0.032	−0.110	−0.027	0.007	0.040	0.086	0.058
MEI	−0.013	0.036	−0.031	−0.031	−0.121	−0.135	−0.078
EASMI	−0.093	−0.068	0.025	0.244	**0.283***	**0.299***	**0.341***

* indicates the significant correlation at a level of α = 0.05.

Table 3
Statistics of extreme precipitation indices in the urban and sub-urban areas.

		UA	ISAN	ISAS	ISA	UA/ISAN	UA/ISAS	UA/ISA
1960–1980	R90pD	6.02	6.19	5.51	5.94	0.97	1.09	1.01
	R95pD	3.13	3.18	3.27	3.20	0.98	0.96	0.98
	R99pD	0.77	0.68	0.77	0.70	1.13	1.00	1.10
	R90pR	0.54	0.53	0.57	0.54	1.02	0.95	1.00
	R95pR	0.38	0.36	0.35	0.35	1.06	1.09	1.09
	R99pR	0.15	0.13	0.14	0.13	1.15	1.07	1.15
1981–2012	R90pD	5.79	5.36	4.43	4.90	1.08	1.31	1.18
	R95pD	2.90	2.66	2.30	2.48	1.09	1.26	1.17
	R99pD	0.51	0.48	0.48	0.48	1.06	1.06	1.06
	R90pR	0.47	0.45	0.45	0.45	1.04	1.04	1.04
	R95pR	0.30	0.29	0.30	0.30	1.03	1.00	1.00
	R99pR	0.09	0.09	0.10	0.09	1.00	0.90	1.00
1960–2012	R90pD	5.88	5.69	4.86	5.31	1.03	1.21	1.11
	R95pD	2.99	2.86	2.69	2.77	1.05	1.11	1.08
	R99pD	0.62	0.56	0.60	0.57	1.11	1.03	1.09
	R90pR	0.50	0.48	0.50	0.49	1.04	1.00	1.02
	R95pR	0.33	0.32	0.32	0.32	1.03	1.03	1.03
	R99pR	0.11	0.10	0.11	0.11	1.10	1.00	1.00

3.4.4. Topographical effects

Many studies have reported that changes in extreme precipitation are associated with elevation changes (Mei et al., 2018; Liu et al., 2013; Chen et al., 2015; Zhang et al., 2014), although the relationships can vary regionally. To investigate the relationship between the extreme precipitation and elevation, we calculated the correlations between extreme indices and the elevations. In this study, the elevation of rain-gauges ranges from 18 to 782 m. The relationships between extreme precipitation indices and elevations, with Pearson's correlation coefficients and statistical significance are shown in Fig. 14. All the frequency indices of extreme precipitation were positively and non-significantly correlated with elevation, with correlation coefficients lower than 0.2. However, all the contribution indices of extreme precipitation were negatively correlated with elevation, with no statistically significant at a level of 0.05. The statistical results of each index in categorized elevation bands are shown in Fig. 15. The largest mean values for all the indices appeared at 100–200 m. All the extreme precipitation indices showed similar fluctuations in value with elevation, where the values increased and then descended with the increase of elevation. Overall, the higher values of precipitation extremes appeared in relatively low-elevation areas. Additionally, in order to further discuss the effect of topography on changes in precipitation extremes, the differences of precipitation extremes between the plain and the mountain areas are also detected. The values of precipitation extremes in the plain areas, located in the southeast of the study area as shown in Fig. 1, are estimated from 25 rain-gauges in this study (NGZ, FHY, BBD, HC, MJQ, YLZ, DHM, LGQ, YAM, LJHY, GBD, TZ, SLZ, YFZ, WQ, SZ, DSGZ, SY, SH, PG, TYK, SSL, TZS, HR and MY). The values in mountain areas are calculated based on the other 35 rain-gauges. The time series of precipitation extremes in the plain and mountain areas are shown in Fig. S2, and the differences between the plain and mountain areas are shown in Fig. 16. The results show that all the mean of the extreme indices except for R90pD in plain areas are larger than that in mountain areas. Interestingly, we find that almost each extreme index in plain areas is larger than that in mountain areas during 1960–1980 whereas most of these indices in plain areas is relatively lower than that in mountain areas during the period of 1981–2012. In conclusion, the changes in precipitation extremes in Beijing are also affected by elevation changes, especially in spatial changes, but these effects have no any statistical significance. Therefore, the further and deeper discussion will be investigated in the future work.

3.5. Implication of extreme precipitation on urban flooding

Cities, as the concentrated representation of human society, are identified among the most vulnerable regions in the context of climate change. In addition, many urban areas are developing rapid population growth and asset accumulation, which further exacerbates the vulnerability of these cities to climate-related extreme events (Tangang et al., 2017). Urban flooding is the major threat to many cities around the world. High frequency urban flooding with more significant impacts on

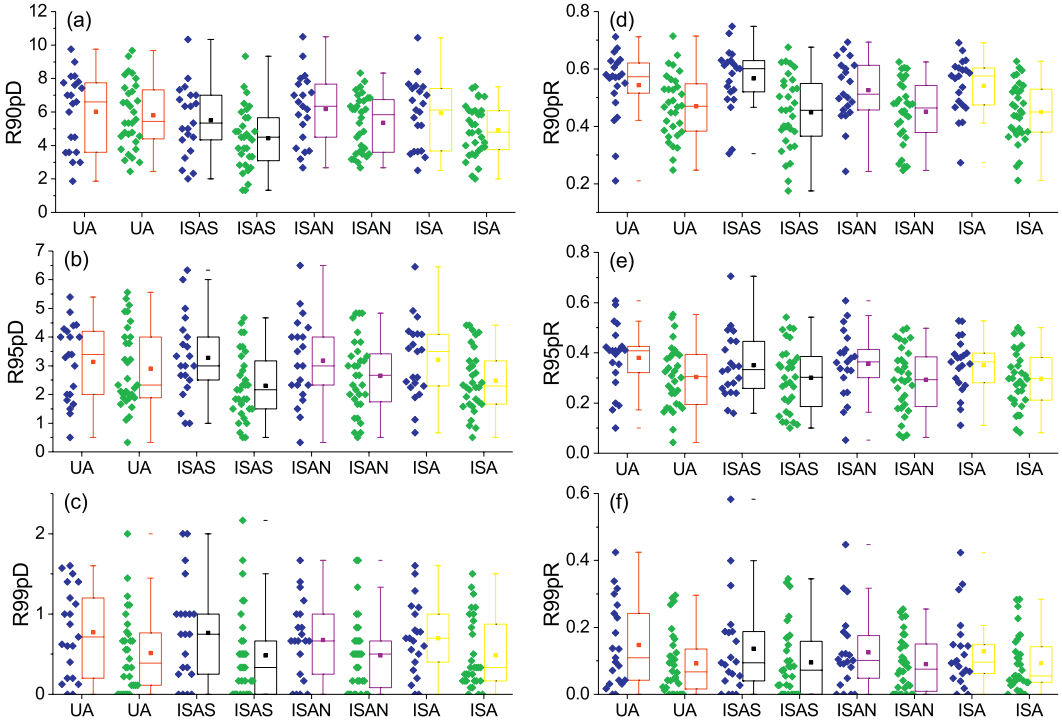

Fig. 13. Box plot of extreme precipitation indices in urban and suburban areas. Blue points represent the dataset during 1960–1980 and green points are the dataset during 1981–2012. (For interpretation of the references to colour in this figure legend, the reader is referred to the web version of this article.)

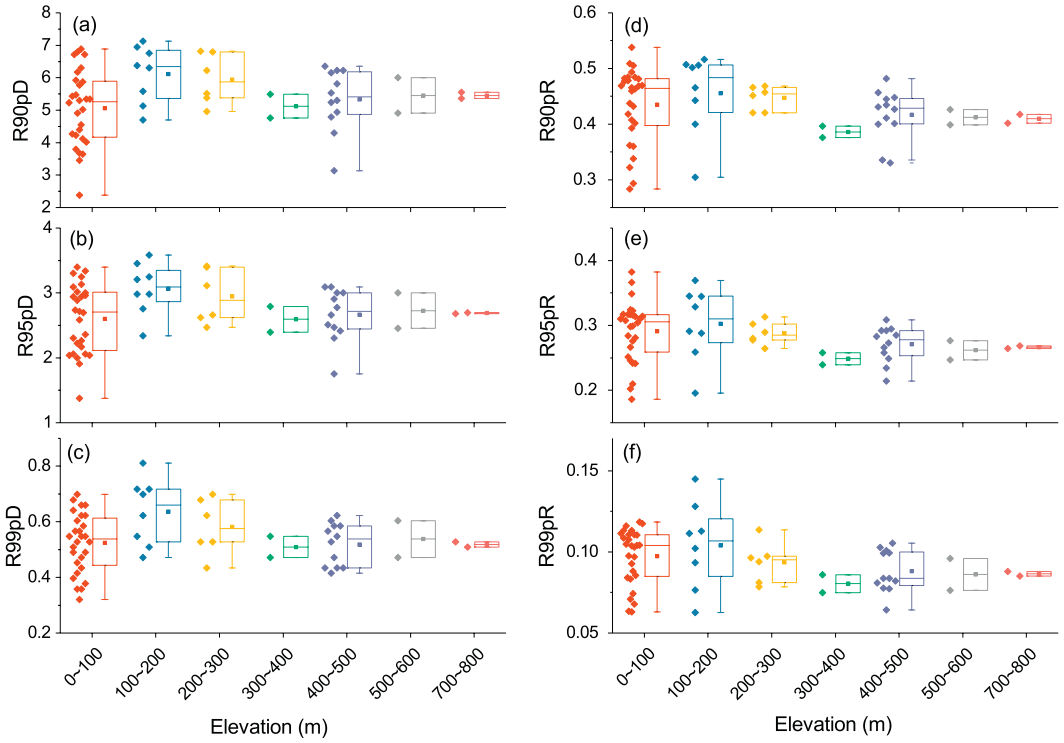

Fig. 14. Correlations between extreme precipitation indices and elevation.

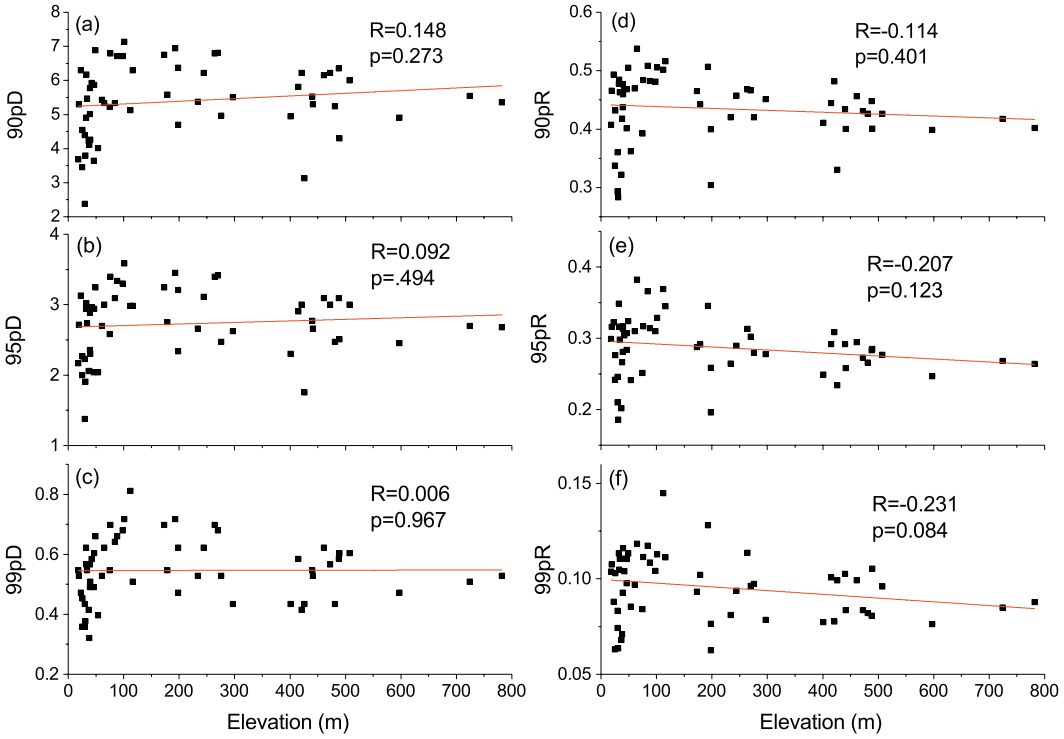

Fig. 15. Box plot of extreme precipitation indices in categorized elevation bands.

developing countries has made it necessary to develop more efficient urban flood management planning (Solaiman et al., 2011). Generally, heavy precipitation, combined with an insufficient sewer system capacity can cause urban flooding.

Recently, more local waterlogging events in Beijing were caused by extreme precipitation events, which has aroused widespread attention by the local community. According to the statistical results released by the Beijing Water Authority, the number of extreme precipitation events with hourly rainfall > 70 mm reached 37 during the period of 2003–2012. However, the areal average annual precipitation is 527.7 mm in 2003–2012 because Beijing suffered a long-term drought from 1999 to 2010. Obviously, the contribution of hourly precipitation to the total precipitation is > 13.3%. This indirectly affects the speed of urban drainage and causes local waterlogging due to a lower drainage

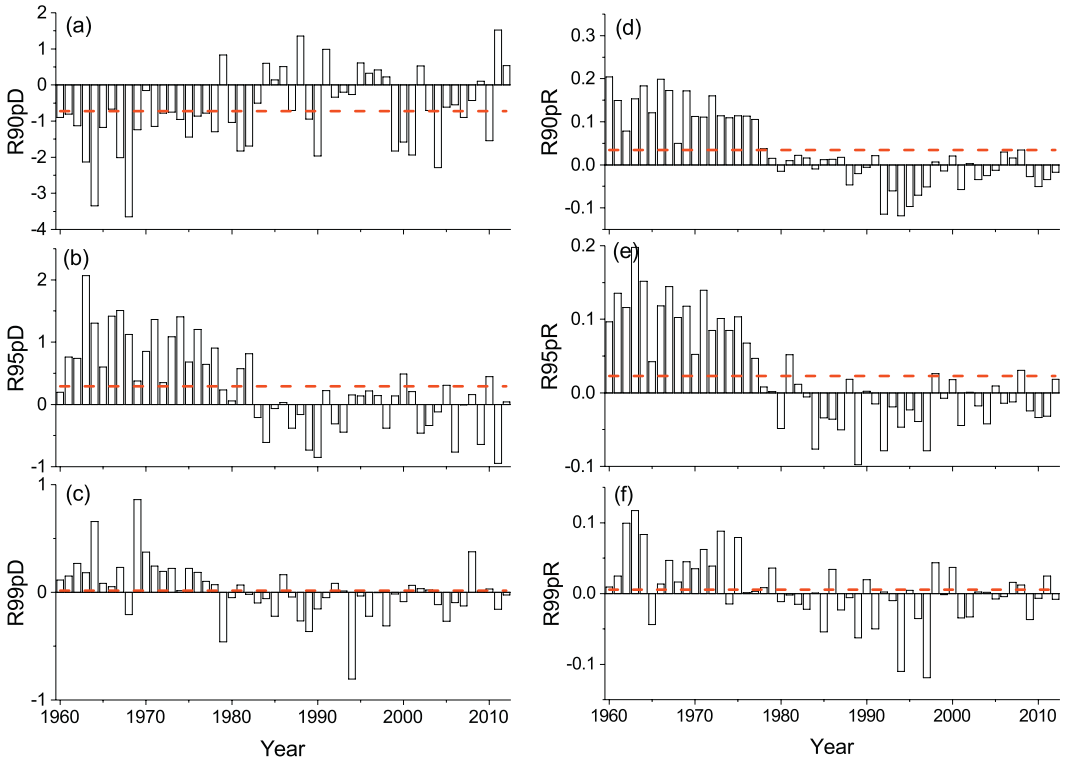

Fig. 16. Time series of the differences in extreme precipitation indices between the plain and mountain areas.

standard (Song et al., 2014). For example, on July 10, 2004, a sudden strong rainstorm hit Beijing. The thunderstorm continued for about three hours with an average of 70 mm in urban areas and a maximum downpour of 106 mm fell on Tiananmen Square. The thunderstorm flooded about 5000 houses and injured three people in addition to causing a traffic jam in the downtown area. Another storm event happened on June 23, 2011, with an average precipitation of 96 mm in southwest Beijing. > 29 bridges and roads were flooded and 3 people died. On July 21, 2012, Beijing experienced one of the heaviest rain events of the past six decades (the area with > 100 mm of rain covered 86% of the whole area of Beijing). The heaviest precipitation, an average of 219 mm the central city, triggered flash floods and landslides that killed 79 people, caused $2 billion in direct economic losses, destroyed at least 8200 homes in the city, and affected > 1.6 million people (Zhang et al., 2013).

Changes in precipitation extremes dramatically affect the design of stormwater management structures. This issue is critical because variations in extreme precipitation may be larger than those of average estimates (Notaro et al., 2015). Therefore, the design criteria for drainage infrastructure requires revision to take into account the expected changes in the intensity and frequency of heavy rainfall events. Due to variations of extreme precipitation characteristics, neglecting their effects in the hydraulic design of urban infrastructure could lead to underestimation or overestimation of design storms. For most severe urban inundations, rainfall often exceed design rainfall values. Therefore, it is necessary to redesign infrastructure systems to drain storm water more efficiently.

4. Conclusions

This study was based on observational data from 60 rain-gauge stations in the Beijing metropolitan area during 1960–2012. Six indices of extreme precipitation were employed to analyze the temporal and spatial distribution characteristics of extreme precipitation using a variety of methods including the minimum cross entropy, wavelet transform coherence method, and the Mann-Kendall test. We examined the frequency and contribution ratio during 1960–2012. The main findings from the study include the following:

(1) Overall, all the extreme precipitation indices showed a decreasing trend across the Beijing area in 1960–2012. A visible negative trend was detected since 1980s, especially during the second half of the 2000s, with a statistically significant trend at a level of $\alpha = 0.05$. The changing point occurs in the middle and late-1990s for the frequency indices, while it appears in 1980 for the contribution ratio indices except for R99pR.
(2) The spatial distributions of extreme precipitation indices are similar to the spatial distribution of annual total precipitation with a more apparent west-east variation pattern, caused by topographical and urbanization effects. An increasing trend for the extreme precipitation indices mostly occurred in urban areas and the southern part of the Beijing Plain area.
(3) The frequency and contribution indices show a decreasing trend during the two periods (1960–1980 and 1981–2012). The rate of change is −3.2%, −8.6% and − 19.8% for the R90pD, R95pD and R99pD, and − 7.32%, −12.67% and − 22.42% for the R90pR, R95pR and R99pR, respectively. But the distribution functions of precipitation have not changed significantly in 1981–2012 relative to 1960–1980.
(4) The extreme precipitation events tend to have more concentrated spatial structure with narrow spatial standard deviations. The frequency indices show more similar spatial and temporal trends relative to total precipitation than the contribution ratio indices.
(5) The changes in precipitation extremes are likely caused by the urban expansion and climate change. The spatial dependence of extreme precipitation events implies a higher probability of simultaneous occurrences of heavy precipitation events across the entire Beijing area. The urban area and the southeast mountainous area will face a relatively higher risk in extreme precipitation and flooding events due to the larger frequency and contribution ratio of extreme precipitation.

Supplementary data to this article can be found online at https://doi.org/10.1016/j.atmosres.2019.02.006.

Acknowledgements

This study was supported by the Fundamental Research Funds for the Central Universities (2015XKMS034), the National Natural Science Foundation of China (51609242), the National Key Research & Development Program of China (2017YFC1502701), the China Postdoctoral Science Foundation (2018M632333), the Open Research Fund Program of State Key Laboratory of Water Resources and Hydropower Engineering Science (2015SWG02) and the Open Research Fund Program of State Key Laboratory of Hydrology-Water Resources and Hydraulic Engineering (2015490411). We are thankful to the Beijing Hydrological Stations (BHC) of the Beijing Water Authority (BWA) for providing precipitation data. We are also thankful to Dr. Linying Cheng for her help in the KL test. The global climate indices can be downloaded from the Earth System Research Laboratory of NOAA (http://www.esrl.noaa.gov/) and the East Asian Monsoon indices from Jianping Li's homepage (http://ljp.gcess.cn/dct/page/65577).

References

AghaKouchak, A., 2014. Entropy-Copula in Hydrology and Climatology. J. Hydrometeorol. 15 (6), 2176–2189.
AghaKouchak, A., Behrangi, A., Sorooshian, S., Hsu, K., Amitai, E., 2011. Evaluation of satellite-retrieved extreme precipitation rates across the central United States. J. Geophys. Res. Atmos. 116.
Ahmad, I., et al., 2018. Spatiotemporal analysis of precipitation variability in annual, seasonal and extreme values over upper Indus River basin. Atmos. Res. 213, 346–360.
Alexander, L.V., et al., 2006. Global observed changes in daily climate extremes of temperature and precipitation. J. Geophys. Res.-Atmos. 111 (D5), 1042–1063.
Ali, H., Mishra, V., 2018. Contributions of Dynamic and Thermodynamic Scaling in Subdaily Precipitation Extremes in India. Geophys. Res. Lett. 45 (5), 2352–2361.
Ali, H., Mishra, V., Pai, D.S., 2014. Observed and projected urban extreme rainfall events in India. J. Geophys. Res.-Atmos. 119 (22), 12621–12641.
Allan, R., Soden, B., 2008. Atmospheric warming and the amplification of precipitation extremes. Science 321 (5895), 1481–1484.
Bonsal, B., Zhang, X., Vincent, L., Hogg, W., 2001. Characteristics of daily and extreme temperatures over Canada. J. Clim. 14 (9), 1959–1976.
Cavalcanti, I.F.A., 2012. Large scale and synoptic features associated with extreme precipitation over South America: a review and case studies for the first decade of the 21st century. Atmos. Res. 118, 27–40.
Chan, J., Zhou, W., 2005. PDO, ENSO and the early summer monsoon rainfall over South China. Geophys. Res. Lett. 32 (8).
Chen, Y., Zhai, P., 2013. Persistent extreme precipitation events in China during 1951-2010. Clim. Res. 57 (2), 143–155.
Chen, W., Feng, J., Wu, R., 2013. Roles of ENSO and PDO in the Link of the East Asian Winter Monsoon to the following Summer Monsoon. J. Clim. 26 (2), 622–635.
Chen, F., Chen, H., Yang, Y., 2015. Annual and seasonal changes in means and extreme events of precipitation and their connection to elevation over Yunnan province, China. Quat. Int. 374 (1), 46–61.
Cheng, L., AghaKouchak, A., 2014. Nonstationary Precipitation Intensity-Duration-Frequency Curves for Infrastructure Design in a Changing Climate. Sci. Rep. 4.
Cheng, L., AghaKouchak, A., Gilleland, E., Katz, R., 2014. Non-stationary extreme value analysis in a changing climate. Clim. Chang. 127 (2), 353–369.
Choi, W., Tareghian, R., Choi, J., Hwang, C., 2014. Geographically heterogeneous temporal trends of extreme precipitation in Wisconsin, USA during 1950-2006. Int. J. Climatol. 34 (9), 2841–2852.
Cui, H.J., Singh, V.P., 2017. Application of minimum relative entropy theory for streamflow forecasting. Stoch. Env. Res. Risk A. 31 (3), 587–608.
Damberg, L., AghaKouchak, A., 2014. Global trends and patterns of drought from space. Theor. Appl. Climatol. 117 (3–4), 441–448.
Ding, Y., 2007. The variability of the Asian summer monsoon. J. Meteorol. Soc. Jpn. 85B, 21–54.
Ding, Y., He, C., 2006. The summer monsoon onset over the tropical eastern Indian Ocean: the earliest onset process of the Asian summer monsoon. Adv. Atmos. Sci. 23 (6), 940–950.
Ding, Y., et al., 2007. Detection, causes and projection of climate change over China: an overview of recent progress. Adv. Atmos. Sci. 24 (6), 954–971.
Ding, Y., Wang, Z., Sun, Y., 2008. Inter-decadal variation of the summer precipitation in East China and its association with decreasing Asian summer monsoon. Part I: Observed evidences. Int. J. Climatol. 28 (9), 1139–1161.
Ding, Y., Sun, Y., Wang, Z., Zhu, Y., Song, Y., 2009. Inter-decadal variation of the summer precipitation in China and its association with decreasing Asian summer monsoon Part II: possible causes. Int. J. Climatol. 29 (13), 1926–1944.
Donat, M.G., Lowry, A.L., Alexander, L.V., O'Gorman, P.A., Maher, N., 2016. More extreme precipitation in the world's dry and wet regions. Nat. Clim. Chang. 6 (5), 508–513.
Dong, Q., Chen, X., Chen, T., 2011. Characteristics and changes of Extreme Precipitation in the Yellow-Huaihe and Yangtze-Huaihe Rivers Basins, China. J. Clim. 24 (14), 3781–3795.
Easterling, D., et al., 2000. Climate extremes: Observations, modeling, and impacts. Science 289 (5487), 2068–2074.
Feng, S., Nadarajah, S., Hu, Q., 2007. Modeling annual extreme precipitation in China using the generalized extreme value distribution. J. Meteorol. Soc. Jpn. 85 (5), 599–613.
Feng, J., Yan, D., Li, C., Gao, Y., Liu, J., 2014. Regional frequency analysis of extreme precipitation after drought events in the Heihe River Basin, Northwest China. J. Hydrol. Eng. 19 (6), 1101–1112.
Frich, P., et al., 2002. Observed coherent changes in climatic extremes during the second half of the twentieth century. Clim. Res. 19 (3), 193–212.
Fu, G., et al., 2013. Temporal variation of extreme rainfall events in China, 1961-2009. J. Hydrol. 487, 48–59.
Gao, T., Xie, L., 2016. Spatiotemporal changes in precipitation extremes over Yangtze River basin, China, considering the rainfall shift in the late 1970s. Glob. Planet. Chang. 147, 106–124.
Gao, M., Mo, D.Y., Wu, X.Q., 2016. Nonstationary modeling of extreme precipitation in China. Atmos. Res. 182, 1–9.
Gao, T., Wang, H.X.J., Zhou, T.J., 2017. Changes of extreme precipitation and nonlinear influence of climate variables over monsoon region in China. Atmos. Res. 197, 379–389.
Gao, L., Huang, J., Chen, X.W., Chen, Y., Liu, M.B., 2018. Contributions of natural climate changes and human activities to the trend of extreme precipitation. Atmos. Res. 205, 60–69.
Georgescu, M., Morefield, P.E., Bierwagen, B.G., Weaver, C.P., 2014. Urban adaptation can roll back warming of emerging megapolitan regions. Proc. Natl. Acad. Sci. USA 111 (8), 2909–2914.
Ghosh, S., Das, D., Kao, S., Ganguly, A., 2012. Lack of uniform trends but increasing spatial variability in observed Indian rainfall extremes. Nat. Clim. Chang. 2 (2), 86–91.
Goswami, U.P., Hazra, B., Goyal, M.K., 2018. Copula-based probabilistic characterization of precipitation extremes over North Sikkim Himalaya. Atmos. Res. 212, 273–284.
Grinsted, A., Moore, J., Jevrejeva, S., 2004. Application of the cross wavelet transform and wavelet coherence to geophysical time series. Nonlinear Process. Geophys. 11 (5–6), 561–566.
Hallegatte, S., Green, C., Nicholls, R.J., Corfee-Morlot, J., 2013. Future flood losses in major coastal cities. Nat. Clim. Chang. 3 (9), 802–806.
Han, L., et al., 2015. Changing properties of precipitation extremes in the urban areas, Yangtze River Delta, China, during 1957-2013. Nat. Hazards 79 (1), 437–454.
Hao, Z., Singh, V.P., 2012. Entropy-copula method for single-site monthly streamflow simulation. Water Resour. Res. 48.
Hao, Z., AghaKouchak, A., Phillips, T.J., 2013. Changes in concurrent monthly precipitation and temperature extremes. Environ. Res. Lett. 8 (3), 034014.
He, J., Wen, M., Ding, Y., Zhang, R., 2006. Possible mechanism of the effect of convection over Asian-Australian "land bridge" on the East Asian summer monsoon onset. Sci. China. Ser. D Earth Sci. 49 (11), 1223–1232.
Janssen, E., Sriver, R.L., Wuebbles, D.J., Kunkel, K.E., 2016. Seasonal and regional variations in extreme precipitation event frequency using CMIP5. Geophys. Res. Lett. 43 (10), 5385–5393.
Jevrejeva, S., Moore, J., Grinsted, A., 2003. Influence of the arctic oscillation and El Nino-Southern Oscillation (ENSO) on ice conditions in the Baltic Sea: the wavelet approach. J. Geophys. Res.-Atmos. 108 (D21).
Kendall, M.G., 1975. Rank Correlation Methods. Griffin, London.
Kenyon, J., Hegerl, G., 2010. Influence of Modes of climate Variability on Global Precipitation Extremes. J. Clim. 23 (23), 6248–6262.
Kishtawal, C.M., Niyogi, D., Tewari, M., Pielke, R.A., Shepherd, J.M., 2010. Urbanization signature in the observed heavy rainfall climatology over India. Int. J. Climatol. 30 (13), 1908–1916.
Kullback, S., Leibler, R.A., 1951. On information and sufficiency. Ann. Math. Stat. 22 (1), 79–87.
Kunkel, K.E., et al., 2012. Meteorological Causes of the Secular Variations in Observed Extreme Precipitation events for the Conterminous United States. J. Hydrometeorol. 13 (3), 1131–1141.
Lenderink, G., Van Meijgaard, E., 2008. Increase in hourly precipitation extremes beyond expectations from temperature changes. Nat. Geosci. 1 (8), 511–514.
Li, J., Zeng, Q., 2002. A unified monsoon index. Geophys. Res. Lett. 29 (8).
Li, Q., Nakatsuka, T., Kawamura, K., Liu, Y., Song, H., 2011. Hydroclimate variability in the North China Plain and its link with El Nino-Southern Oscillation since 1784 AD: Insights from tree-ring cellulose delta O-18. J. Geophys. Res.-Atmos. 116.
Li, Z., Yan, Z.W., Tu, K., Wu, H.Y., 2015. Changes of precipitation and extremes and the possible effect of urbanization in the Beijing Metropolitan Region during 1960-2012 based on Homogenized Observations. Adv. Atmos. Sci. 32 (9), 1173–1185.
Liang, P., Ding, Y.H., 2017. The long-term variation of extreme heavy precipitation and its link to Urbanization Effects in Shanghai during 1916-2014. Adv. Atmos. Sci. 34 (3), 321–334.
Liu, Y., Ding, Y., 2008. Analysis and Numerical Simulations of the Teleconnection between Indian Summer Monsoon and Precipitation in North China. Acta Meteorol. Sinica 22 (4), 489–501.
Liu, W.L., et al., 2013. Changes in precipitation extremes over Shaanxi province, northwestern China, during 1960-2011. Quat. Int. 313-314 (10), 118–129.
Liu, Z., et al., 2014. Chinese cave records and the East Asia Summer Monsoon. Quat. Sci. Rev. 83, 115–128.
Mann, H.B., 1945. Nonparametric tests against trend. Econometrica 13, 245–259.
Mei, C., et al., 2018. Multi-decadal spatial and temporal changes of extreme precipitation

patterns in northern China (Jing-Jin-Ji district, 1960-2013). Quat. Int. 476, 1–13.
Min, S., Zhang, X., Zwiers, F., Hegerl, G., 2011. Human contribution to more-intense precipitation extremes. Nature 470 (7334), 378–381.
Mishra, A.K., Ozger, M., Singh, V.P., 2009. An entropy-based investigation into the variability of precipitation. J. Hydrol. 370 (1–4), 139–154.
Mishra, V., Dominguez, F., Lettenmaier, D.P., 2012. Urban precipitation extremes: how reliable are regional climate models? Geophys. Res. Lett. 39.
Mishra, V., Ganguly, A.R., Nijssen, B., Lettenmaier, D.P., 2015. Changes in observed climate extremes in global urban areas. Environ. Res. Lett. 10 (2).
Niu, J., Sivakumar, J., Sivakumar, B., 2014. Teleconnection analysis of runoff and soil moisture over the Pearl River basin in southern China. Hydrol. Earth Syst. Sci. 18 (4), 1475–1492.
Notaro, V., Liuzzo, L., Freni, G., La Loggia, G., 2015. Uncertainty Analysis in the Evaluation of Extreme Rainfall Trends and its Implications on Urban Drainage System Design. Water-Sui 7 (12), 6931–6945.
Ouyang, R., et al., 2014. Linkages between ENSO/PDO signals and precipitation, streamflow in China during the last 100 years. Hydrol. Earth Syst. Sci. 18 (9), 3651–3661.
Pakalidou, N., Karacosta, P., 2018. Study of very long-period extreme precipitation records in Thessaloniki, Greece. Atmos. Res. 208, 106–115.
Pingale, S.M., Khare, D., Jat, M.K., Adamowski, J., 2014. Spatial and temporal trends of mean and extreme rainfall and temperature for the 33 urban centers of the arid and semi-arid state of Rajasthan, India. Atmos. Res. 138, 73–90.
Ren, G., et al., 2012. Recent progress in studies of climate change in China. Adv. Atmos. Sci. 29 (5), 958–977.
Rosenzweig, C., Solecki, W., Hammer, S.A., Mehrotra, S., 2010. Cities lead the way in climate-change action. Nature 467 (7318), 909–911.
Sang, Y.F., Singh, V.P., Hu, Z.Y., Xie, P., Li, X.X., 2018. Entropy-aided evaluation of meteorological droughts over China. J. Geophys. Res.-Atmos. 123 (2), 740–749.
Singh, V.P., 2011. Hydrologic synthesis using entropy theory: review. J. Hydrol. Eng. 16 (5), 421–433.
Siswanto, S., van Oldenborgh, G.J., van der Schrier, G., Jilderda, R., van den Hurk, B., 2016. Temperature, extreme precipitation, and diurnal rainfall changes in the urbanized Jakarta city during the past 130 years. Int. J. Climatol. 36 (9), 3207–3225.
Solaiman, T.A., King, L.M., Simonovic, S.P., 2011. Extreme precipitation vulnerability in the Upper Thames River basin: uncertainty in climate model projections. Int. J. Climatol. 31 (15), 2350–2364.
Song, X.M., et al., 2014. Rapid urbanization and changes in spatiotemporal characteristics of precipitation in Beijing metropolitan area. J. Geophys. Res.-Atmos. 119 (19), 11250–11271.
Soon, W., et al., 2014. A review of Holocene solar-linked climatic variation on centennial to millennial timescales: Physical processes, interpretative frameworks and a new multiple cross-wavelet transform algorithm. Earth Sci. Rev. 134, 1–15.
Sun, W.Y., et al., 2016. Changes in extreme temperature and precipitation events in the Loess Plateau (China) during 1960-2013 under global warming. Atmos. Res. 168, 33–48.
Tabari, H., Willems, P., 2018. Lagged influence of Atlantic and Pacific climate patterns on European extreme precipitation. Sci. Rep. 8.
Tangang, F., et al., 2017. Characteristics of precipitation extremes in Malaysia associated with El Nino and La Nina events. Int. J. Climatol. 37, 696–716.
Tedeschi, R.G., Grimm, A.M., Cavalcanti, I.F.A., 2016. Influence of Central and East ENSO on precipitation and its extreme events in South America during austral autumn and winter. Int. J. Climatol. 36 (15), 4797–4814.
Thapa, K., Endreny, T.A., Ferguson, C.R., 2018. Atmospheric Rivers Carry Nonmonsoon Extreme Precipitation into Nepal. J. Geophys. Res.-Atmos. 123 (11), 5901–5912.
Thiombiano, A.N., El Adlouni, S., St-Hilaire, A., Ouarda, T.B.M.J., El-Jabi, N., 2017. Nonstationary frequency analysis of extreme daily precipitation amounts in Southeastern Canada using a peaks-over-threshold approach. Theor. Appl. Climatol. 129 (1–2), 413–426.
Tong, S.Q., et al., 2019. Spatial and temporal variability in extreme temperature and precipitation events in Inner Mongolia (China) during 1960-2017. Sci. Total Environ. 649, 75–89.
Torrence, C., Webster, P., 1999. Interdecadal changes in the ENSO-monsoon system. J. Clim. 12 (8), 2679–2690.
Touma, D., Michalak, A.M., Swain, D.L., Diffenbaugh, N.S., 2018. Characterizing the Spatial Scales of Extreme Daily Precipitation in the United States. J. Clim. 31 (19), 8023–8037.
Wang, Y., Zhou, L., 2005. Observed trends in extreme precipitation events in China during 1961-2001 and the associated changes in large-scale circulation. Geophys. Res. Lett. 32 (9).
Wang, B., et al., 2008a. How to measure the strength of the East Asian summer monsoon. J. Clim. 21 (17), 4449–4463.
Wang, W., Chen, X., Shi, P., van Gelder, P., 2008b. Detecting changes in extreme precipitation and extreme streamflow in the Dongjiang River Basin in southern China. Hydrol. Earth Syst. Sci. 12 (1), 207–221.
Wang, W., et al., 2012. SPATIO-temporal variation of seasonal extreme wet days in China and its relationship with SST anomalies. J. Trop. Meteorol. 18 (4), 485–493.
Wang, F., Yang, S., Higgins, W., Li, Q., Zuo, Z., 2014. Long-term changes in total and extreme precipitation over China and the United States and their links to oceanic-atmospheric features. Int. J. Climatol. 34 (2), 286–302.
Wang, X.L., Hou, X.Y., Wang, Y.D., 2017. Spatiotemporal variations and regional differences of extreme precipitation events in the Coastal area of China from 1961 to 2014. Atmos. Res. 197, 94–104.
Wei, W., Chang, Y., Dai, Z., 2014. Streamflow changes of the Changjiang (Yangtze) river in the recent 60 years: Impacts of the East Asian summer monsoon, ENSO, and human activities. Quat. Int. 336, 98–107.
Wibig, J., Piotrowski, P., 2018. Impact of the air temperature and atmospheric circulation on extreme precipitation in Poland. Int. J. Climatol. 38 (12), 4533–4549.
Willems, P., 2013. Revision of urban drainage design rules after assessment of climate change impacts on precipitation extremes at Uccle, Belgium. J. Hydrol. 496, 166–177.
Wu, H.T.J., Lau, W.K.M., 2016. Detecting climate signals in precipitation extremes from TRMM (1998–2013)Increasing contrast between wet and dry extremes during the "global warming hiatus". Geophys. Res. Lett. 43 (3), 1340–1348.
Wu, B., Zhang, R., Ding, Y., D'Arrigo, R., 2008. Distinct modes of the East Asian summer monsoon. J. Clim. 21 (5), 1122–1138.
Wu, W.J., Zhao, S.Q., Zhu, C., Jiang, J.L., 2015. A comparative study of urban expansion in Beijing, Tianjin and Shijiazhuang over the past three decades. Landscape Urban Plan 134, 93–106.
Xie, Z., Du, Y., Zeng, Y., Miao, Q., 2018. Classification of yearly extreme precipitation events and associated flood risk in the Yangtze-Huaihe River Valley. Sci China Earth Sci 61 (9), 1341–1356.
Xu, M., et al., 2006. Steady decline of east Asian monsoon winds, 1969–2000: evidence from direct ground measurements of wind speed. J. Geophys. Res. 111 (D24).
Yang, L., Smith, J., 2018. Sensitivity of Extreme Rainfall to Atmospheric Moisture Content in the Arid/Semiarid Southwestern United States: Implications for Probable Maximum Precipitation estimates. J. Geophys. Res.-Atmos. 123 (3), 1638–1656.
Yao, C., Qian, W., Yang, S., Lin, Z., 2010. Regional features of precipitation over Asia and summer extreme precipitation over Southeast Asia and their associations with atmospheric-oceanic conditions. Meteorog. Atmos. Phys. 106 (1–2), 57–73.
Ye, J., 2014. Trend and variability of China's summer precipitation during 1955-2008. Int. J. Climatol. 34 (3), 559–566.
You, Q., et al., 2011. Changes in daily climate extremes in China and their connection to the large scale atmospheric circulation during 1961-2003. Clim. Dyn. 36 (11－12), 2399–2417.
Zarekarizi, M., Rana, A., Moradkhani, H., 2018. Precipitation extremes and their relation to climatic indices in the Pacific Northwest USA. Clim. Dyn. 50 (11–12), 4519–4537.
Zhai, P., Zhang, X., Wan, H., Pan, X., 2005. Trends in Total Precipitation and Frequency of Daily Precipitation Extremes over China. J. Clim. 18 (7), 1096–1108.
Zhang, D.L., et al., 2013. The Beijing extreme rainfall of 21 July 2012: "Right results" but for wrong reasons. Geophys. Res. Lett. 40 (7).
Zhang, K., et al., 2014. Spatial distribution and temporal trends in precipitation extremes over the Hengduan Mountains region, China, from 1961 to 2012. Quat. Int. 349, 346–356.
Zhang, D.D., Yan, D.H., Wang, Y.C., Lu, F., Liu, S.H., 2015. GAMLSS-based nonstationary modeling of extreme precipitation in Beijing-Tianjin-Hebei region of China. Nat. Hazards 77 (2), 1037–1053.
Zhang, Z.X., Li, N., Wang, X., Liu, F., Yang, L.P., 2016. A Comparative Study of Urban expansion in Beijing, Tianjin and Tangshan from the 1970s to 2013. Remote Sens-Basel 8 (6).
Zhao, Y., Zhang, Q., Du, Y., Jiang, M., Zhang, J., 2013. Objective Analysis of Circulation Extremes during the 21 July 2012 Torrential rain in Beijing. Acta Meteorologica Sinica 27 (5), 626–635.
Zhao, J., Yu, K., Li, D., 2014a. Spatial characteristics of local floods in Beijing urban area. Urban Water J. 11 (7), 557–572.
Zhao, Y., Zou, X., Cao, L., Xu, X., 2014b. Changes in precipitation extremes over the Pearl River Basin, southern China, during 1960-2012. Quat. Int. 333, 26–39.
Zheng, J., Wang, W., Ge, Q., Man, Z., Zhang, P., 2006. Precipitation variability and extreme events in eastern China during the past 1500 years. Terrestrial Atmospheric Oceanic Sci. 17 (3), 579–592.
Zhou, X.Y., Lei, W.J., 2018. Complex patterns of precipitation and extreme events during 1951-2011 in Sichuan Basin, Southwestern China. J. Mt Sci-Engl 15 (2), 340–356.
Zhou, X., Ding, Y., Wang, P., 2010. Moisture Transport in the Asian Summer Monsoon Region and its Relationship with Summer Precipitation in China. Acta Meteorol. Sinica 24 (1), 31–42.
Zhou, X., Bai, Z., Yang, Y., 2017. Linking trends in urban extreme rainfall to urban flooding in China. Int. J. Climatol. 37 (13), 4586–4593.
Zolina, O., et al., 2014. Precipitation Variability and Extremes in Central Europe New View from STAMMEX results. Bull. Am. Meteorol. Soc. 95 (7), 995–1002.